REPORT DOCUMENTATION PAGE

AFRL-SR-BL-TR-01-

0064

Public reporting burden for this collection of information is estimated to average 1 hour per response including the time for review data needed and completing and reviewing this collection of information. Send comments regarding this burden estimate or any this burden to Department of Defense Washington Headquarters Services Directorate for Information Operations and Reports ((4302 Respondents should be aware that notwithstanding any other provision of law no person shall be subject to any penalty fr valid OMB control number PLEASE DO NOT RETURN YOUR FORM TO THE ABOVE ADDRESS.

1. REPORT DATE (DD-MM-YYYY)	2. REPORT TYPE	3. DATES COVERED
27-11-2000	Final Technical Report	6/15/96-11/14/98

4. TITLE AND SUBTITLE

Assembly of Ge Quantum-Dots on Silicon: Applications to Nanoelectronics

5a. CONTRACT NUMBER

5b. GRANT NUMBER
F49620-96-1-0313

5c. PROGRAM ELEMENT NUMBER

6. AUTHOR(S)

Dr. Mohan Krishnamurthy

5d. PROJECT NUMBER

5e. TASK NUMBER
C757/03, C757/05, C757/09

5f. WORK UNIT NUMBER

7. PERFORMING ORGANIZATION NAME(S) AND ADDRESS(ES)

Michigan Technological University
1400 Townsend Drive
Houghton, MI 49931-1295

8. PERFORMING ORGANIZATION REPORT NUMBER

9. SPONSORING / MONITORING AGENCY NAME(S) AND ADDRESS(ES)

AFOSR/NE
110 Duncan Avenue Room B115
Bolling AFB, DC 20332-8050

10. SPONSOR/MONITOR'S ACRONYM(S)

11. SPONSOR/MONITOR'S REPORT NUMBER(S)

12. DISTRIBUTION / AVAILABILITY STATEMENT

APPROVED FOR PUBLIC RELEASE,
DISTRIBUTION UNLIMITED

AIR FORCE OFFICE OF SCIENTIFIC RESEARCH (AFOSR)
NOTICE OF TRANSMITTAL DTIC. THIS TECHNICAL REPORT
HAS BEEN REVIEWED AND IS APPROVED FOR PUBLIC RELEASE
LAW AFR 190-12. DISTRIBUTION IS UNLIMITED.

13. SUPPLEMENTARY NOTES

14. ABSTRACT

There are four publications related to this project. They are entitled as follows:

1. Microstructural Development and Optical Properties of Epitaxial GE1-xCX Alloys on Si(100)
2. The Ge-C Local Mode in Epitaxial GeC and Ge-rich GeSiC Alloys
3. Incorporation and Stability of Carbon During Low-Temperature Epitaxial Growth of Ge1-xCx (x less than 0.1) Alloys on Si(100): Microstructural and Raman Studies
4. Low-temperature Epitaxial Growth of Ge-Si-C Alloys: Microstructure, Raman Studies, and Optical Properties.

15. SUBJECT TERMS

20010220 015

16. SECURITY CLASSIFICATION OF:			17. LIMITATION OF ABSTRACT	18. NUMBER OF PAGES	19a. NAME OF RESPONSIBLE PERSON
a. REPORT	b. ABSTRACT	c. THIS PAGE			19b. TELEPHONE NUMBER (include area code)

The Ge–C local mode in epitaxial GeC and Ge-rich GeSiC alloys

W. H. Weber[a)]
Physics Department, MD-3028/SRL, Ford Motor Company, Dearborn, Michigan 48121-2053

B.-K. Yang and M. Krishnamurthy
Department of Metallurgical and Materials Engineering, Michigan Technological University, Houghton, Michigan 49931

(Received 19 January 1998; accepted for publication 27 May 1998)

The Raman signature of the local Ge–C mode for substitutional C is identified as a narrow line (8 cm^{-1} full width at half maximum) near 530 cm^{-1} in alloy films of $Ge_{1-y}C_y$ ($0 \leq y \leq 0.07$) grown on Ge (100) substrates by low-temperature (200 °C) molecular beam epitaxy. The intensity of the Ge–C line relative to the *c*-Ge line suggests that only a small fraction of the nominal C is in substitutional sites. In ternary alloys of $Ge_{1-x-y}Si_xC_y$ with $x=0.1$ and 0.2 and $y=0.03$, the Ge–C mode disappears, suggesting a strong bias towards C bonding with Si as opposed to Ge. In $Ge_{1-x}Sn_x$ films the Ge–Sn mode is seen at 263 cm^{-1}. © *1998 American Institute of Physics.* [S0003-6951(98)00231-9]

The addition of small amounts of C to the Ge–Si alloy system is considered an attractive method for reducing the lattice-constant mismatch in layered growth of band gap engineered materials.[1] The introduction of C also offers an extra degree of freedom to tune the electronic properties by varying both strain and composition. Although the solubility of substitutional C in bulk Si or Ge is extremely low,[2] the solubility near a surface can be several orders of magnitude higher,[3] which offers the possibility of producing metastable films with super-saturated concentrations as high as 2–3 at. %.[4] Thin-film samples with concentrations this high have been achieved by a variety of techniques including molecular beam epitaxy (MBE)[5–8] and chemical vapor deposition.[9–11]

In Si and Si-rich alloys, substitutional C produces a characteristic Si–C local Raman mode at 605 cm^{-1}.[5,6,12–15] Observations of this mode are significant, since they confirm the presence of substitutional C, as opposed to interstitial or surface C, and they yield microscopic information regarding the distribution of C in the lattice.[12,15–18] The mode intensity can be used to estimate the absolute concentration of substitutional C, and the satellite structure around the main peak can indicate the occurrence of preferential instead of random second or third nearest-neighbor C–C spacings.

In this letter we report on the corresponding Ge–C local mode in Ge and Ge-rich alloys. Although the existence of this mode has been anticipated in several recent papers,[6,13,19,20] and its position even tentatively assigned, it has not been unequivocally identified due to its extreme weakness in Si-rich alloys or because of interference with other Raman features from the film or the substrate. As with the Si–C local mode, observations of the Ge–C mode confirm the presence of substitutional C and shed light on the microscopic C distribution. The latter feature is particularly important in the Ge–Si–C alloys, since Kelires has shown that Ge–C bonds are energetically unfavorable compared with Si–C or Ge–Si bonds, so that highly nonrandom distributions can be expected.[21]

The samples in this study are epitaxial films of $Ge_{1-x-y}Si_xC_y$ alloys, nominally 50–70 nm thick, grown on Ge (100) substrates using a Riber 32 MBE system with base pressure lower than 5×10^{-10} mbar as described in more detail elsewhere.[20] The films were analyzed *in situ* by reflection high-energy electron diffraction (RHEED) and *ex situ* by x-ray diffraction (XRD), transmission electron microscopy (TEM), and atomic force microscopy (AFM). Rutherford backscattering (RBS) was used to calibrate the various Ge, Si, and C sources. The Ge(100) substrates were degreased and cleaned in de-ionized water and then In-bonded to a Mo block. The oxide was desorbed *in situ* at 500–550 °C and a 20-nm Ge buffer layer was grown at ~1 nm/min and 200 °C substrate temperature. A sharp (2×1) RHEED pattern from clean Ge was observed in all samples. The Si was deposited either from a Knudsen source with a TaC crucible or from a rod-fed electron beam source. The C was deposited from a rod-fed electron beam source, whose flux was varied to control the C concentration. The ratio of this flux to that of the Ge flux we refer to as the "nominal" C concentration.

During codeposition of the Ge and C (and Si, in the case of SiGeC growth), the RHEED pattern undergoes significant changes. For all samples the (2×1) pattern transforms gradually to a (1×1) pattern followed by three-dimensional island formation and strong {311} faceting during later stages of growth. The higher the C concentration, the sooner these changes occur. Plan-view and cross-sectional TEM images of the 5%C Ge–C film have already been reported.[20] The plan-view images show strain contrast with no indications of dislocations. Cross-sectional views show {311} facets decorated with C clusters. AFM images of the surface show uniformly distributed islands of average size ~ 50 nm and heights of 10 nm or less, which is consistent with the TEM results. Attempts to determine the film's lattice parameter by 2θ XRD scans showed no clear evidence of a peak from the epilayer separate from the strong Ge substrate signal.

Raman spectra were obtained using a Renishaw 1000 Raman microscope with 633 nm excitation. At this wavelength the films are sufficiently transparent that their Raman signals are comparable to those from the substrate. Since the

a)Electronic mail: wweber3@ford.com

 © 1998 American Institute of Physics

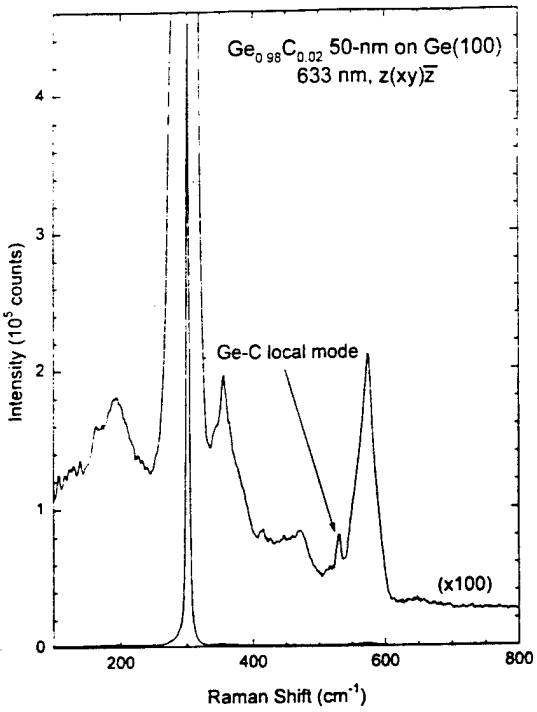

FIG. 1. Raman spectrum of a 50 nm thick, GeC alloy film with nominal 2% C concentration. Experimental conditions: 3 mW and 20 min exposure.

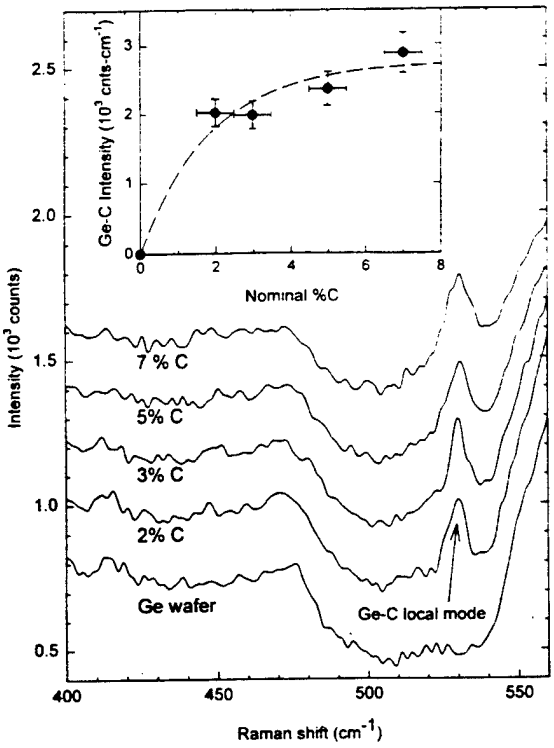

FIG. 2. Spectra of films with different C concentrations and a pure Ge wafer recorded under identical conditions as those for Fig. 1. Successive spectra are shifted up by 200 counts for clarity. The inset shows the integrated intensity of the Ge–C local mode vs nominal %C. The dashed line is a fit to $a(1-\exp\{-bx\})$ drawn as a guide to the eye.

Ge–C local mode occurs near the crystalline Si (c-Si) line at 521 cm^{-1}, it is crucial that we use a Ge substrate. In all of our spectra taken earlier on Si substrates, the c-Si line completely obscures the much weaker Ge–C local mode.[20]

Figure 1 shows the Raman spectrum from a 50 nm thick $Ge_{1-y}C_y$ epilayer with a nominal C concentration of 2%. The spectrum is recorded with $z(xy)\bar{z}$ scattering geometry, for which the first-order c-Ge line and the Ge–C local mode are allowed and the second-order scattering is largely suppressed. In the magnified plot, the broad feature peaking near 575 cm^{-1} is the second-order band from the Ge optical branch. All the features in this spectrum, excepting the narrow line at 530 cm^{-1}, indicated in the figure, also appear in the spectrum from a pure Ge (100) wafer. We assign this extra line to the Ge–C local mode. This line is absent from the Ge-wafer spectrum, and its strength increases with C content. It follows the same selection rules as the c-Ge peak, i.e., it is observed in xy and $x'x'$ scattering and is quenched in xx and $x'y'$ scattering. In addition, its frequency is consistent with that expected from the known position of the Si–C local mode at 605 cm^{-1}. Compared with the Si–C mode, the larger reduced mass of the Ge–C pair will shift the frequency down to $\sim$546 cm^{-1}, which corresponds to a factor $(m_{Si\text{-}C}/m_{Ge\text{-}C})^{1/2}$, where the m_{i-j}'s are reduced masses ($m_{i-j}^{-1}=m_i^{-1}+m_j^{-1}$). The further downward shift of $\sim$3% is likely caused by the larger lattice constant for Ge compared with Si, which increases the Ge–C bond length and decreases the force constant.

The Ge–C mode in Fig. 1 has a full width at half maximum of 8 cm^{-1}. The narrowness of this mode is consistent with its frequency—well above the top of the one-phonon continuum and just below the overtone band from the c-Ge optical branch, in a region where the second-order scattering is weak.[22] Thus, one-phonon decay processes are forbidden and two-phonon processes should be very weak.

Figure 2 shows an expanded plot of the Ge–C line for samples with different C content along with a Ge-wafer spectrum. The linewidth increases about 25% at the highest C concentration, but the integrated line strength, shown in the inset, increases by only about 50%. This result suggests that the substitutional C content saturates at a value well below the concentration expected from the growth process.

There are also subtle changes in the c-Ge parts of the spectrum as well. The first-order peak broadens slightly ($\sim$10%) and decreases in integrated intensity ($\sim$20%), and the structure on the edges and near the peaks of the second-order features tends to become less sharp. These effects are likely caused by the faceting and reduction in long-range order inherent in the growth process. Unfortunately, these changes make it impossible to form difference spectra between C-doped and pure Ge samples without introducing extra structure throughout the region below 600 cm^{-1}.

We observe a broad band, peaking near 1400 cm^{-1}, that increases with C content. This band is the signature for amorphous C (a-C),[20,23] indicating that at least some of the extra C goes into a-C. There are also additional weak, sharp lines in the spectra (near 950 and 1050 cm^{-1}) of unknown origin, which may be related to specific C or Ge–C clusters.

In GeSiC alloy films with 10% and 20% Si and nominally 3% C, we find the usual Ge–Ge and Ge–Si lines, but we find no evidence for the Ge–C local mode. A likely explanation for this effect is that the strong preference for C to form Si–C bonds leads to every C being paired with a Si atom.[21]

In $Si_{1-y}C_y$ alloys Meléndez-Lira *et al.*[19] found that the ratio of integrated intensities of the Si–C mode at 605 cm^{-1}

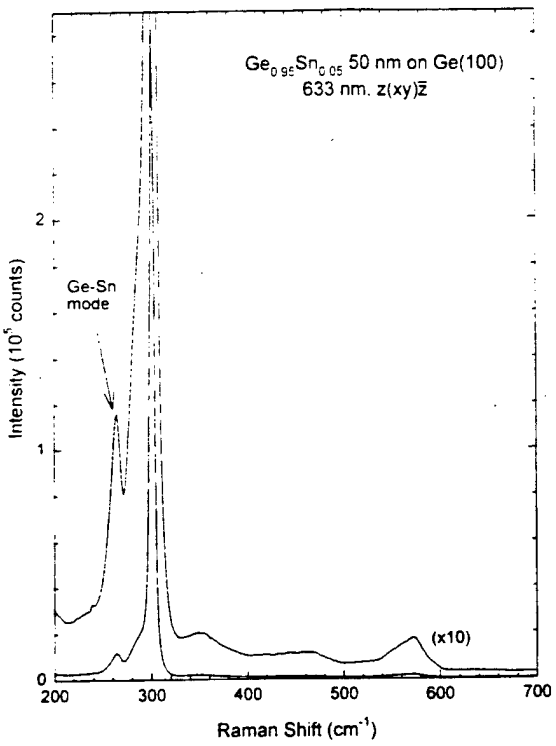

FIG. 3. Raman spectrum of a GeSn epilayer with nominal 5% Sn, recorded under the same conditions as for Fig. 1.

to the c-Si line at 521 cm^{-1} was given by $\sim 3.7y$, where y is the substitutional C fraction. A theoretical estimate of this ratio yielded $1.9y$, which is within a factor of 2 of the experimental result. If we apply the same theoretical arguments they used to estimate the corresponding ratio between the Ge–C and c-Ge modes, we predict a ratio $\sim 2.6y$ for our samples. Our measured ratio for the nominal 2% C sample of Fig. 1 is 8×10^{-4}, which is nearly two orders of magnitude smaller than the predicted value of 5×10^{-2}. We conclude either that there is a strong resonant enhancement of the c-Ge mode relative to the Ge–C mode or the substitutional C concentration is extremely small. A resonance enhancement cannot be ruled out, since the 633 nm laser excitation is near the E_1 critical point of the c-Ge electronic response. However, it is worth noting that the C concentration suggested by the Raman intensity ratio, $\sim 3\times10^{-4}$, would imply (using Vegard's law) a tensile strain of $\sim 1\times10^{-4}$, which would be too small by about a factor of 10 to be detectable in our x-ray studies.

As a check on the validity of using Raman intensity ratios to estimate dopant concentrations in Ge, we examined a 50 nm thick Ge–Sn alloy film grown in the same fashion as the Ge–C films. In a Ge lattice it is generally easier to get Sn into a substitutional site than C.[24,25] The Raman spectrum for a nominal 5% Sn alloy is shown in Fig. 3. The Ge–Sn vibration is identified as the peak at 263 cm^{-1}, and, as expected, there is no suggestion of a peak in the 450–550 cm^{-1} region. The integrated intensity ratio of this line to the c-Ge line is 5×10^{-2}, which is the same order of magnitude as the nominal Sn fraction, and which is consistent with the results on the Si–C mode in $Si_{1-y}C_y$ alloys.[19] This result supports the conclusion that our substitutional C concentration is well below the nominal C fraction.

The Ge–Sn mode is not truly "local" in the same sense as the Ge–C mode. Since Sn is heavier than Ge, the Ge–Sn vibrations will strongly mix with the continuum from the Ge optical branch, resulting in a much broader line. As evidence of this mixing, the relative linewidth ($\Delta\omega/\omega$) for the Ge–Sn mode is $\sim 3\times$ larger than that for the Ge–C mode.

In summary, we have identified the Ge–C local mode in $Ge_{1-y}C_y$ epitaxial films on Ge (100) substrates as a sharp line at 530 cm^{-1}. The intensity of this line relative to the c-Ge line and its variation with C content suggest that the substitutional C concentration is well below the nominal C fraction. At least some of the extra C appears in the Raman spectra as a-C. In GeSiC alloys the Ge–C line disappears, indicating a strong preference for the formation of Si–C bonds as opposed to Ge–C bonds.

The authors wish to thank Barry Wilkens (Arizona State University) for RBS measurements. Financial support for part of this research (M.K. and B.Y.) has been provided by the Office of Naval Research (N00014-96-1-0793).

[1] R. A. Soref, Proc. IEEE **81**, 1687 (1993).
[2] *Physics of Group IV Elements and III-V Compounds*, edited by K.-H. Hellwege and O. Madelung, Landolt-Börnstein, New Series, Group III, Vol. 17, Part A (Springer, Berlin, 1982).
[3] J. Tersoff, Phys. Rev. Lett. **74**, 5080 (1995).
[4] H. J. Osten, Mater. Sci. Eng., B **36**, 268 (1996).
[5] S. S. Iyer, K. Eberl, M. S. Goorsky, F. K. LeGoues, J. C. Tsang, and F. Cardone, Appl. Phys. Lett. **60**, 356 (1992).
[6] H. J. Osten, E. Bugiel, and P. Zaumseil, J. Cryst. Growth **142**, 322 (1994).
[7] J. Kolodzey, P. A. O'Neil, S. Zhang, B. A. Orner, K. Roe, K. M. Unruh, C. P. Swann, M. M. Waite, and S. I. Shah, Appl. Phys. Lett. **67**, 1865 (1995).
[8] M. Krishnamurthy, B.-K. Yang, and W. H. Weber, Appl. Phys. Lett. **69**, 2572 (1996).
[9] Z. Atzmon, A. E. Bair, E. J. Jaquez, J. W. Mayer, D. Chandrasekhar, D. J. Smith, R. L. Hervig, and McD. Robinson, Appl. Phys. Lett. **65**, 2559 (1994).
[10] J. L. Regolini, S. Bodnar, J. C. Oberlin, F. Ferrieu, M. Gauneau, B. Lambert, and P. Boucaud, J. Vac. Sci. Technol. A **12**, 1015 (1994).
[11] M. Todd, J. Kouvetakis, and D. J. Smith, Appl. Phys. Lett. **68**, 2047 (1996).
[12] M. Meléndez-Lira, J. D. Lorentzen, J. Menéndez, W. Windl, N. G. Cave, R. Liu, J. W. Christiansen, N. D. Theodore, and J. J. Candelaria, Phys. Rev. B **56**, 3648 (1997).
[13] J. C. Tsang, K. Eberl, S. Zollner, and S. S. Iyer, Appl. Phys. Lett. **61**, 961 (1992).
[14] B. Dietrich, H. J. Osten, H. Rücker, M. Methfessel, and P. Zaumseil, Phys. Rev. B **49**, 17 185 (1994).
[15] H. Rücker and M. Methfessel, Phys. Rev. B **52**, 11 059 (1995).
[16] H. Rücker, M. Methfessel, B. Dietrich, K. Pressel, and H. J. Osten, Phys. Rev. B **53**, 1302 (1996).
[17] M. Meléndez-Lira, J. Menéndez, W. Windl, O. F. Sankey, G. S. Spencer, S. Sego, R. B. Culbertson, A. E. Bair, and T. F. Alford, Phys. Rev. B **54**, 12 866 (1996).
[18] L. Simon, K. Kubler, J. Groenen, and J. L. Balladore, Phys. Rev. B **56**, 9947 (1997).
[19] M. Meléndez-Lira, J. Menéndez, K. M. Kramer, M. O. Thompson, N. Cave, R. Liu, J. W. Christiansen, N. D. Theodore, and J. J. Candelaria, J. Appl. Phys. **82**, 4246 (1997).
[20] B.-K. Yang, M. Krishnamurthy, and W. H. Weber, J. Appl. Phys. **82**, 3287 (1997).
[21] P. C. Kelires, Phys. Rev. Lett. **75**, 1114 (1995).
[22] B. A. Weinstein and M. Cardona, Phys. Rev. B **7**, 2545 (1973).
[23] J. E. Smith, M. H. Brodsky, B. L. Crowder, and M. I. Nathan, J. Non-Cryst. Solids **8–10**, 179 (1972).
[24] W. Wegscheider, J. Olajos, U. Menczigar, W. Dondl, and G. Abstreiter, J. Cryst. Growth **123**, 75 (1992).
[25] M. E. Taylor, G. He, H. A. Atwater, and A. Polman, J. Appl. Phys. **80**, 4383 (1996).

Microstructural development and optical properties of epitaxial $Ge_{1-x}C_x$ alloys on Si(100)

M. Krishnamurthy,[a] Bi-Ke Yang, and W. H. Weber[b]
Department of Metallurgical and Materials Engineering, Michigan Technological University, Houghton, Michigan 49931

(Received 10 July 1996; accepted for publication 26 August 1996)

We report on the microstructural development and optical properties of epitaxial $Ge_{1-x}C_x$ alloys ($0<x<0.1$) grown on Si(100) by low-temperature (200 °C) molecular-beam epitaxy. Films with C concentrations below 2%–3% grow in 2D layers, while films with C higher than 5% form 3D islands after initial layer growth. X-ray-diffraction indicates that less than 1% C may have been substitutionally incorporated. Spectroscopic ellipsometry measurements of the films' optical constants show small systematic changes with increasing C concentration. These changes occur primarily near 2 eV, the E_1 critical point in Ge. No new features attributable to Ge–C vibrational modes could be identified using Raman spectroscopy. © *1996 American Institute of Physics.* [S0003-6951(96)04943-1]

Silicon–germanium alloys have been studied in order to exploit the promise of new devices obtainable by "band-gap engineering" on silicon.[1] Recently, there has been an increasing interest in SiGe alloys containing carbon.[2] One of the reasons for substitutionally alloying with C is that (assuming Vegard's law) approximately a 9:1 Ge:C ratio will lattice match SiGeC alloys to Si, circumventing critical thickness limitations inherent in SiGe technology. However, the relative insolubility of C in both Si and Ge and the precipitation of various forms of SiC at higher growth temperatures[3] are obstacles to the fabrication of these alloys. Despite these problems, low concentrations of substitutional C in the alloys have been successfully incorporated using a variety of techniques including chemical-vapor deposition (CVD)[4,5] and molecular-beam epitaxy (MBE).[6–9]

The Ge–C system is an alternative pathway for Si-based band-gap engineering. In addition to the fact that it is a simpler binary system, problems associated with compound formation can be avoided since no stable GeC phase exists. Several researchers have reported on the growth of Ge_xC_{1-x} alloys[8–11] on Si. Previous MBE studies of Ge_xC_{1-x} films were typically performed at higher temperatures (600 °C) on Ge buffers[8] or using Sb surfactants,[9] with little emphasis on microstructural development or the dielectric function. Our earlier study of $Ge_{1-x}C_x$ epitaxy on Si had shown that high-C films (>20%) grown at room temperature and annealed at higher temperatures formed 3D islands and the Ge and C were phase separated.[11]

In this letter, we report on MBE growth of $Ge_{1-x}C_x$ alloys on Si(100) at 200 °C, for C concentrations between 0% and 10%. The films were characterized *in situ* by reflection high-energy electron diffraction (RHEED) and *ex situ* by transmission electron microscopy (TEM), x-ray diffraction, Raman spectroscopy, and spectroscopic ellipsometry (SE).

The $Ge_{1-x}C_x$ films were grown in a Riber 32 MBE system with base pressure better than 5×10^{-10} mbar. Si(100) substrates were chemically cleaned and oxidized by boiling in a H_2O_2:H_2SO_4 mixture. After the sample had been degassed in the MBE chamber at ~200 °C overnight, the oxide was desorbed by heating to just below 900 °C for about 15 min. Sharp (2×1) diffraction spots indicative of a clean surface were typically observed in RHEED (in some cases a couple of monolayers of Ge were deposited on the oxide before desorption to produce a better quality surface). Germanium was deposited from a previously calibrated pyrolytic boron nitride Knudsen source at ~10 Å/min. The C was deposited from a rod-fed electron-beam source, and the flux was varied to obtain various C concentrations. Rutherford backscattering spectroscopy (RBS) (including C resonance) was used to measure the C concentrations. An experiment consisted of the following steps. After the sample had stabilized at ~200 °C (±25 °C), the Ge shutter was first opened followed by the C shutter after a 10–30 s delay. The nominal thickness of most films was ~50 nm.

During deposition of the Ge–C alloy, the RHEED pattern undergoes changes depending on the C content, as shown in Figs. 1(a)–1(d). At low C concentrations (0%–2%), the (2×1) reconstruction is stable and the streakiness is indicative of a 2D layer growth with an atomically rough surface [Figs. 1(a) and 1(b)]. For medium C films (3%–5%), the initial 8–10 monolayers (ML); (1 ML=1.4 Å) shows a streaky (2×1) pattern, followed by evidence of transmission spots indicative of 3D island growth [Fig. 1(c)]. For higher C films, extra spots indicative of twinning are also apparent in the RHEED pattern [Fig. 1(d)], and the films tend to become polycrystalline at the later stages of growth.

Figures 2(a) and 2(b) are cross-sectional TEM images of Ge–C films with low C concentration (1%–2% C). Figure 2(a) (~1% C film) shows that the film is of good epitaxial quality with the majority of the misfit defects localized near the interface. The high-resolution image in Fig. 2(b) (~2% C) shows the Ge–C/Si interface with misfit defects, a few planar defects (twins, stacking faults), and localized regions of the lattice where the fringes appear disordered. Figures 3(a) and 3(b) show plan-view and high-resolution cross-sectional TEM images, respectively, of a 50-nm-thick, Ge–C alloy with ~5% C. The plan-view image [Fig. 3(a)] indicates that the film is relaxed with short interfacial misfit disloca-

[a]Electronic mail: mohan@mtu.edu
[b]Physics Department, Ford Research Laboratories, Dearborn, MI 48121.

 0003-6951/96/69(17)/2572/3/$10.00 © 1996 American Institute of Physics

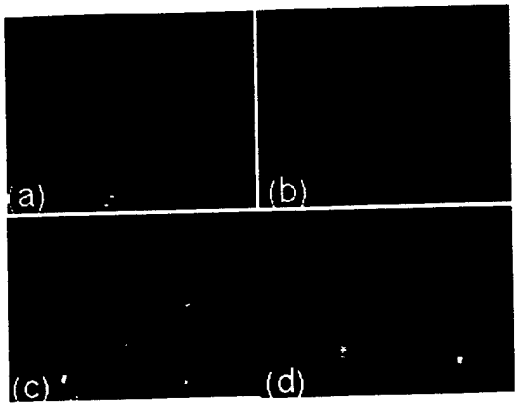

FIG. 1. Typical RHEED patterns observed for (a) pure Ge film, (b) film with <2% C, (c) film with ~5% C showing transmission spots, and (d) film with ~10% C showing twinning spots.

tions as evidenced by the presence of moiré fringes and from weak-beam dark-field images (not shown). The cross-sectional image shows faceting that is consistent with the RHEED observation of 3D islanding. There is no clear evidence for the formation of C clusters or precipitates.

X-ray 2Θ scans were obtained in the (400) range of Si and Ge. The ratio of d_{400Ge}/d_{400Si} is used as a measure of the lattice parameter of the relaxed film, and is plotted as a function of C concentration in Fig. 4. A marginal decrease in the Ge lattice parameter with increasing nominal C concentration is observed. It is estimated (based on Vegard's law) that on an average, a maximum of ~1% C may have been substitutionally incorporated in the films under the growth conditions studied.

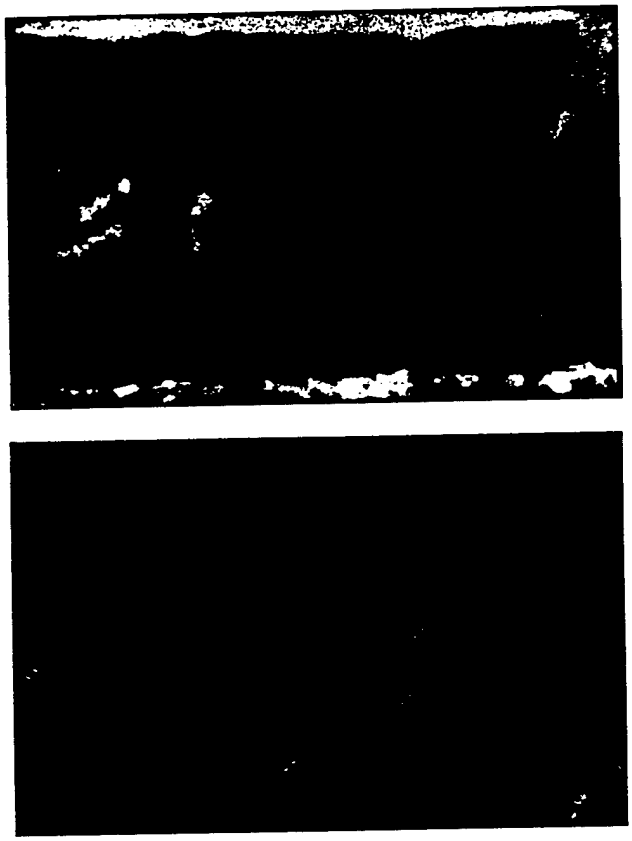

FIG. 2. High-resolution cross-sectional TEM images of $Ge_{1-x}C_x$ films taken along a (110) zone for (a) film with nominally ~1% C and (b) film with ~2% C. Arrows indicate the position of the Ge–C/Si interface.

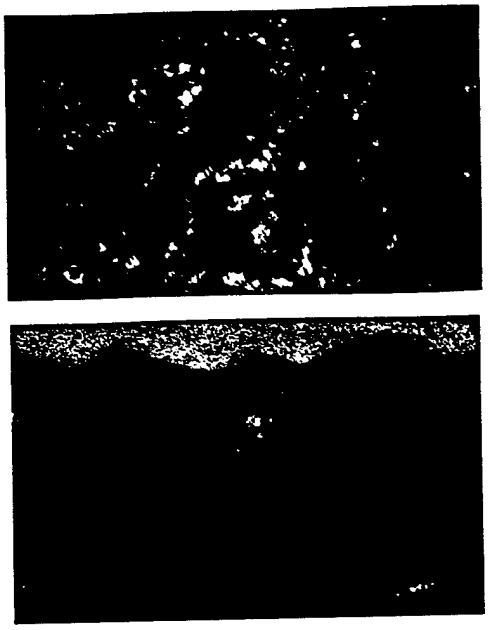

FIG. 3. (a) Plan-view and (b) cross-sectional TEM images of a 5% C, Ge–C film on Si. The plan-view image was taken under two-beam bright-field conditions and shows uniform moiré fringes.

Spectroscopic ellipsometry (SE) measurements were performed on the $Ge_{1-x}C_x$ samples using a variable-angle instrument from J. A. Woollam Co. Data were obtained at five equally spaced angles of incidence from 60° to 80° and over a spectral range of 250–1000 nm. The data were analyzed to extract the optical constants of the films using a three-layer model: Si substrate, $Ge_{1-x}C_x$ layer, and GeO_2 layer. The free parameters were the optical constants and thicknesses of the $Ge_{1-x}C_x$ film and the thicknesses of the GeO_2 layer. The GeO_2 index was determined to be ~1.8 from a separate analysis on pure Ge wafers, and the optical constants of Si were taken from Palik.[12] The free parameters were first fit in the long-wavelength region (λ>680 nm) where there is no sharp structure, by modeling the film optical constants with a Cauchy formula for the real part of the index n and an Urbach tail for the absorption coefficient k.[13] The thicknesses resulting from the fit were then constrained and the optical constants of the film were found for the full wavelength region. This procedure was developed using pure

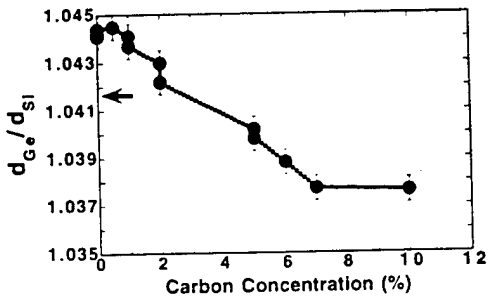

FIG. 4. The ratio of the (400) interplanar spacing of Ge to Si (d_{Ge}/d_{Si}) plotted as a function of nominal C content. The arrow indicates the ratio for an ideally relaxed pure Ge film on Si. Ratios lower than this value correspond to a reduction in the average lattice parameter of the film due to C.

Ge epitaxial layers (with 40–50 Å of oxide) for which it was found to give good agreement with the results of Aspnes and Studna[14] for bulk Ge.

The most pronounced systematic effect of the C alloying is a reduction in the strength of the feature near the E_1 critical point (~2 eV), which is shown in Fig. 5. The solid lines give the real and imaginary dielectric constants for pure Ge. The circles, boxes, and triangles are the data from films with nominal C concentration ~1%, 2%, and 5%, respectively. In addition, less systematic shifts and broadenings also occur at higher energies near the E_2 critical point.

Raman scattering studies were performed on the Ge–C films using 633 and 785 nm lasers. All spectra show the first- and second-order structure from crystalline Si and Ge. No new features attributable to Ge—C bonds could be identified. In the samples with 5% C, the Ge first-order line near 300 cm^{-1} showed some broadening, which may result from the disorder. In fact, the changes in the electronic structure shown in Fig. 5 may result indirectly from an increase in the disorder or local strain in the Ge lattice caused by the C, rather than from a direct interaction with the C orbitals.

There are several interesting aspects of microstructural evolution of the $Ge_{1-x}C_x$ films. It is well understood that pure Ge grown on Si forms islands (after initial layer growth) in order to reduce its strain energy at the cost of increased surface area. By maintaining a sufficiently low substrate temperature (e.g., 200 °C), the reduced surface diffusion of Ge suppresses island formation,[15] as confirmed by Fig. 1(a).

However, it is seen in our study that the presence of C>2%–3% leads to 3D island formation [Fig. 1(c)] even at this low substrate temperature. There are several possible reasons for the increased islanding tendency in Ge–C films. The most obvious one is an increase in the substrate temperature due to radiative heating from the C source. This is unlikely because the thermocouple reading from the substrate registers no significant change during the course of the experiment. Other possibilities include changes in the surface energy of Ge:C, enhancement of surface diffusion kinetics or a combination of both. While further studies are needed to clarify the mechanism, we observe that the growth of Ge–C on a relaxed Ge film at higher substrate temperatures also leads to islanding. We therefore suggest that the increased driving force for island formation in Ge–C films at 200 °C may be due to changes in surface energy (i.e., a nonwetting behavior) induced by the presence of C.

A second microstructural feature associated with increased C concentration is the appearance of twinning in the islands [Fig. 1(d)]. The mechanism for twinning appears to be related to the evolution of islands on the surface and may be due to the misfits associated with island coalescence.[16] It is interesting to note that the microstructural development in Ge–C films (i.e., layer, island, twinned island) is qualitatively similar to the epitaxial growth of another "immiscible" system: Ge–Sn on InSb.[17]

In summary, we show that on Si at 200 °C, epitaxial $Ge_{1-x}C_x$ alloys with C<2%–3% grow in 2D layers, while films with C>5% form 3D islands after initial layer growth. X-ray diffraction indicates that less than 1% C may be substitutionally incorporated in the films. Spectroscopic ellipsometry shows a C-related change in the optical constants near 2 eV (the E_1 critical point in Ge) while Raman spectroscopy shows no Ge–C-related vibrational modes.

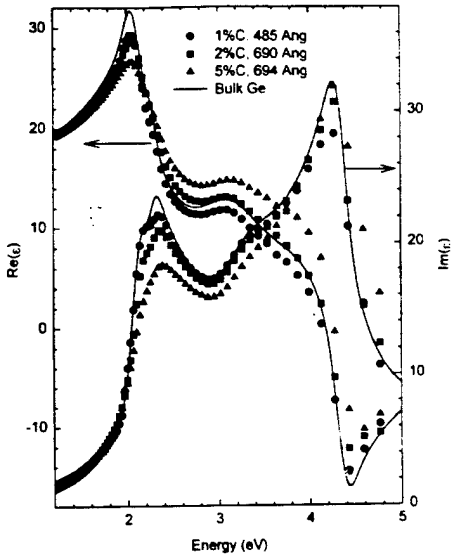

FIG. 5. Plot of the real Re(ϵ) and the imaginary Im(ϵ) parts of the dielectric function of $Ge_{1-x}C_x$ as a function of energy for 1% C (circles), 2% C (squares), and 5% C (triangles) compared with pure Ge (solid line). Observe a systematic change with C concentration near ~2 eV (E_1 critical point in Ge).

We wish to thank Barry Wilkens (ASU) for the RBS measurements, Ed Laitila for technical help, and Professor J. K. Lee for useful discussions. Financial support for this research was provided in part by the Office of Naval Research (N00014-96-1-0793).

[1] See for example, J. C. Bean, Proc. IEEE **80**, 571 (1992); T. P. Pearsall, Crit. Rev. Solid State Mater. Sci. **15**, 551 (1989).
[2] For a review see R. A. Soref, Proc. IEEE **81**, 1687 (1993).
[3] A. R. Powell, F. K. LeGoues, and S. S. Iyer, Appl. Phys. Lett. **64**, 324 (1994).
[4] Z. Atzmon, A. E. Bair, E. J. Jaquez, J. W. Mayer, D. Chandrasekhar, D. J. Smith, R. L. Hervig, and McD. Robinson, Appl. Phys. Lett. **65**, 2559 (1994).
[5] J. L. Regolini, S. Bodnar, J. C. Oberlin, F. Ferrieu, M. Gauneau, B. Lambert, and P. Boucaud, J. Vac. Sci. Technol. A **12**, 1015 (1994).
[6] S. S. Iyer, K. Eberl, M. S. Goorsky, F. K. LeGoues, J. C. Tsang, and F. Cardone, Appl. Phys. Lett. **60**, 356 (1992).
[7] K. Eberl, S. S. Iyer, S. Zollner, J. C. Tsang, and F. K. LeGoues, Appl. Phys. Lett. **60**, 3033 (1992).
[8] J. Kolodzey, P. A. Oneill, S. Zhang, B. A. Orner, K. Roe, K. M. Unruh, C. P. Swann, M. M. Waite, and S. I. Shah, Appl. Phys. Lett. **67**, 1865 (1995).
[9] H. J. Osten, E. Bugiel, and P. Zaumseil, J. Cryst. Growth **142**, 322 (1994).
[10] M. Todd, J. Kouvetakis, and D. J. Smith, Appl. Phys. Lett. **68**, 2407 (1996).
[11] M. Krishnamurthy, J. S. Drucker, and A. Challa, J. Appl. Phys. **78**, 7070 (1995).
[12] *Handbook of Optical Constants*, edited by E. D. Palik (Academic, New York, 1985).
[13] See, for example, *Guide to Using WVASE32*, (J. A. Woolam Co., 1995).
[14] D. E. Aspnes and A. A. Studna, Phys. Rev. B **27**, 985 (1983).
[15] D. J. Eaglesham and M. Cerullo, Appl. Phys. Lett. **58**, 2276 (1991).
[16] See, for example, M. J. Stowell, in *Epitaxial Growth, Part B*, edited by J. W. Matthews (Academic, New York, 1975).
[17] E. A. Fitzgerald, P. E. Freeland, M. T. Asom, W. P. Lowe, R. A. Macharrie, B. E. Weir, A. R. Kortan, F. A. Thiel, Y.-H. Xie, A. M. Sargent, S. L. Cooper, G. A. Thomas, and L. C. Kimmerling, J. Electron. Mater. **20**, 489 (1991).

Incorporation and stability of carbon during low-temperature epitaxial growth of $Ge_{1-x}C_x$ ($x<0.1$) alloys on Si(100): Microstructural and Raman studies

B.-K. Yang and M. Krishnamurthy[a)]
Department of Metallurgical and Materials Engineering, Michigan Technological University, Houghton, Michigan 49931

W. H. Weber
Department of Physics, Ford Research Laboratories, Dearborn, Michigan, 48121

(Received 25 April 1997; accepted for publication 25 June 1997)

Low-temperature (~200 °C) molecular beam epitaxy of $Ge_{1-x}C_x$ alloys grown on Si(100) have been extensively investigated by *in situ* reflection high-energy electron diffraction, *ex situ* x-ray diffraction, transmission electron microscopy, and Raman spectroscopy. Carbon concentrations were nominally varied from 0 up to ~10 at. %. Selected samples were annealed in an Ar ambient at 750 °C to evaluate the stability of the thin films. A few films were also grown on Ge substrates. With increasing C concentration, the epitaxial growth mode changes from two dimensional layer growth to three dimensional island growth. The surface has a tendency to facet along {311} planes under certain growth conditions. The microstructure shows an increase in planar defect density with increasing C concentration. The x-ray diffraction data show that the lattice parameter decreases with increasing C concentration and that a maximum of 1 at. % C is incorporated substitutionally in Ge. Raman spectroscopy shows no clear Ge–C signal though extra intensity is measured at the energies where Ge–C modes may be expected. Films with nominal C concentrations greater than 2 to 3 at. % show clear evidence for amorphous C. We propose that under our growth conditions, nominal C in excess of about 2 to 3 at. % remains on the surface as amorphous C and plays an important role in 3D islanding, defect formation, and {311} faceting during epitaxial growth. © *1997 American Institute of Physics.* [S0021-8979(97)03719-5]

I. INTRODUCTION

Silicon–germanium alloys have been widely studied in order to explore the promise of band gap engineering on silicon.[1] More recently, there has been a strong interest in SiGe alloys containing C.[2] The main reason is that the addition of suitable amounts of C (a ratio 9:1 Ge:C assuming Vegard's law) is expected to lattice match GeSiC to Si, circumventing the critical thickness limitations inherent in SiGe technology. Furthermore, it is possible to use both alloy concentration and strain as a variable for band gap engineering. However, there are problems associated with the fabrication of these alloys. These include: (i) the relative insolubility of C in both Si and Ge and (ii) the precipitation of various forms of SiC at higher growth temperatures.[3] Despite these problems, low concentrations of substitutional C in the alloys have been successfully incorporated using a variety of techniques.[4–7] Current research efforts focus on techniques to increase the amount of substitutional C in the alloys. For example, it has been reported that changes in growth conditions (e.g., growth rates) may change the substitutional-to-interstitial carbon ratio in Si–C alloys.[8,9] Most of the epitaxial growth studies have been limited to Si–C or Si–Ge–C systems.[10]

The Ge–C system is an alternative pathway for Si- based band gap engineering. In addition to the fact that it forms a model binary system, problems associated with compound formation can be avoided since no stable GeC phase is known to exist. Low concentrations of C have been successfully incorporated using molecular beam epitaxy (MBE)[11,12] and chemical vapor deposition.[13] Previous MBE studies of $Ge_{1-x}C_x$ alloys were typically performed at higher temperatures (400–600 °C) on Ge buffers[12] or using Sb surfactants,[11] with little emphasis on understanding the microstructural development or the growth mechanisms in this "immiscible" system. Furthermore, the nominal C content of the alloys in these studies was limited to $x<0.03$.

We have recently reported on the microstructural evolution and optical properties of $Ge_{1-x}C_x$ alloys ($0<x<0.1$) grown on Si at 200 °C.[14,15] Here we report on a systematic study of Ge–C alloys grown on Si as well as on Ge substrates, and the effect of annealing at higher temperatures. Microstructural characterization using electron and x-ray diffraction and electron microscopy is correlated with optical characterization using Raman spectroscopy. The incorporation and stability of C in the films and the influence of C on the epitaxial growth mechanisms are discussed.

II. EXPERIMENTS

The $Ge_{1-x}C_x$ ($0<x<10$ at. %) films were grown in a Riber 32 MBE system with base pressure better than 5×10^{-10} Torr. The 2 in. Si(100) wafers were chemically cleaned and oxidized by boiling in a H_2O_2:H_2SO_4 mixture followed by rinsing in deionized water before being loaded into the MBE chamber. After the sample had been degassed in the MBE chamber at ~200 °C overnight, the oxide was

a)Electronic mail: mohan@mtu.edu

 0021-8979/97/82(7)/3287/10/$10.00 © 1997 American Institute of Physics

desorbed by heating to just below 900 °C for about 15 min. Sharp (2×1) diffraction spots indicative of a clean surface were typically observed in reflection high-energy electron diffraction (RHEED). In some cases, a couple of monolayers of Ge were deposited on the oxide before desorption to produce a better quality surface. Germanium was deposited from a previously calibrated pyrolytic boron nitride Knudsen source at ~1 nm/min. The C was deposited from a rod-fed electron-beam source, and the flux was varied to obtain various C concentrations up to 10 at. %. Rutherford backscattering spectroscopy (including C resonance) was used to estimate the C concentrations (with error less than ~0.5 at. %). A typical experiment consisted of the following steps. After the sample had stabilized at ~200 °C, the Ge shutter was first opened followed by the C shutter after a 10–30 s delay. The nominal thickness of $Ge_{1-x}C_x$ films was ~50 nm.

In addition to the regular samples discussed above, three samples (called A, B, and C) were fabricated under similar growth conditions (i.e., 200 °C substrate temperature). Sample A had a ~50-nm-thick Ge–C (5% C) thin film grown on Si(100) and subsequently capped with ~50 nm Ge. Sample B was a Ge–C (5% C) film grown on Si(100) and capped with ~20-nm-thick Si. Sample C was a ~50-nm-thick Ge–C (5% C) film grown on a Ge(100) substrate. The Ge substrate was prepared by cleaning in deionized water followed by oxide desorption in the MBE chamber at ~500 °C. In addition, a ~20-nm-thick Ge buffer was grown at 200 °C to give a sharp (2×1) reconstructed Ge surface.

Selected samples were annealed at 750 °C for about 1 h in an Ar ambient to evaluate the stability of the thin films. Most of the thin films were characterized *ex situ* by transmission electron microscopy (TEM) and x-ray diffraction (XRD). The x-ray 2θ scans were performed in a Siemens D500 diffractometer system using Cu $K\alpha$ radiation. TEM samples were prepared by conventional mechanical polishing followed by ion milling at liquid nitrogen temperatures. The microscopy was performed in JEOL 100cx or 4000fx microscopes.

Raman spectroscopy was also performed on most samples. The Raman spectra were obtained with a Renishaw 1000 Raman microscope using the 633 nm HeNe laser for excitation. This instrument has holographic optics to reject the Rayleigh scattering, a CCD array detector, and a single stage spectrometer. The laser power was typically 4 to 5 mW; a 50x objective was used, giving a spot size of a few μm's; exposure times were typically 5 min, giving ~10^5 counts on the strongest lines; and the spectral resolution [full width at half maximum (FWHM)] was 4.7 cm^{-1}, as measured on a series of plasma emission lines used for calibration. There is sufficient transmission in our films at 633 nm so that all spectra showed the sharp *c*-Si line near 520 cm^{-1} from the substrate. This line gave a convenient reference to check the reproducibility of our frequency-shift measurements. Over a period of several days, the *c*-Si line from a dozen samples was found to occur at 521.30±0.08 cm^{-1}, where the uncertainty is one standard deviation. The *c*-Ge peak measured at the same time from a Ge wafer was at 301.70 cm^{-1}.

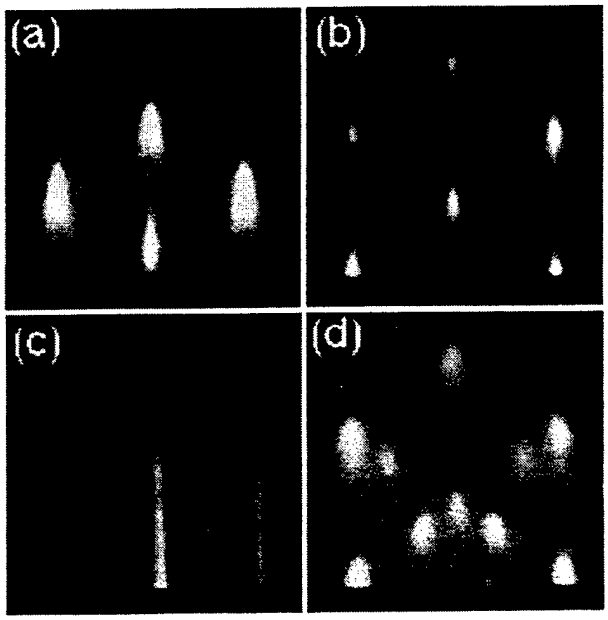

FIG. 1. RHEED patterns showing: (a) 3D island formation for Ge–C(5%) films on Si, (b) pronounced faceting of the islands (in the first few monolayers) when Ge is deposited on Ge–C(5%) layer, (c) continued Ge deposition leading to a smooth 2D layer, and (d) tendency to form twinning defects when Si is deposited on Ge–C(5%).

III. RESULTS

A. RHEED patterns

For $Ge_{1-x}C_x$ thin films grown on Si, the observed evolution of RHEED patterns depends on the carbon content, as reported previously.[14] The general tendency is that at low C concentrations ($x<2$ to 3 at. %), the (2×1) reconstruction is stable and a streaky pattern indicative of a 2D layer growth is observed on the surface. For medium C films ($x=3-5$ at. %), the initial 8–10 ML's (1 ML=1.4 Å) show a streaky (2×1) pattern, followed by evidence of transmission spots indicative of 3D island growth. For even higher C films, extra spots indicative of twinning were also observed.

Figure 1(a)–(d) shows RHEED patterns observed during the growth of samples A and B. Figure 1(a) is the typical RHEED pattern of Ge–C (5% C) films grown on Si(100). It is noted that the pattern shows transmission spots indicative of 3D growth. In addition, the spots show a chevron making a maximum angle with the {100} plane of ~10°. Figure 1(b) is also a pattern from sample A, but after the first few MLs of pure Ge have been deposited on the Ge–C surface. Strong streaks indicative of facet formation on the 3D islands were immediately observed. The angle between the main {100} and the facet plane is ~20°, consistent with {411} type facets. With continued Ge deposition, this feature gradually changed to a sharp (2×1) streaky pattern, as shown in Fig. 1(c). For sample B, however, when Si was deposited on the Ge–C layer at 200 °C, the RHEED pattern continued to show the 3D transmission spots and further developed some extra spots indicating the formation of twins, as shown in Fig. 1(d). For sample C, Ge–C thin films on Ge(100) substrates, strong faceting developed after the first few monolayers of codeposition of Ge and C, and became more pro-

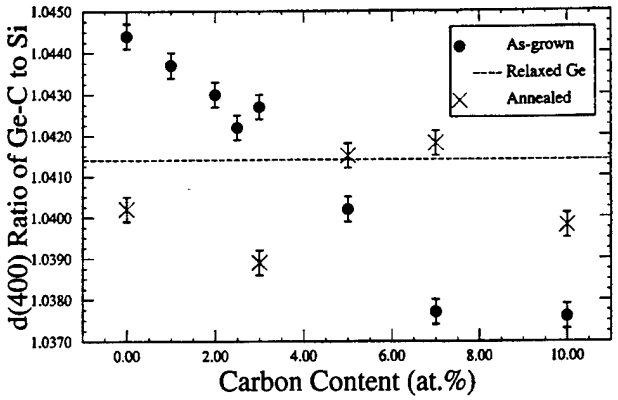

FIG. 2. The d_{400} ratio of the Ge–C films to the Si substrates obtained from XRD, plotted against the C concentration. Notice the decrease of lattice parameter with increased C content for as-grown films. After anneal, there is some decrease in lattice parameter for C<3% alloys and some increase for C=5%–10% alloy films relative to the as-grown films. The dashed line indicates the value for relaxed bulk Ge.

nounced upon further deposition. The facet streaks were measured to be from {311} type planes.[15]

B. X-ray diffraction results

X-ray diffraction 2θ scans were performed on all the as-grown and annealed samples. To minimize the systematic errors, the Ge–C(400) peak positions were normalized with that of the Si(400) substrate peak position. In other words, the ratio of d_{400} of Ge–C to Si was calculated from the peak positions. This d ratio is plotted as a function of carbon concentration, as shown in Fig. 2. The dashed line indicates the ideal ratio of the relaxed bulk Ge to that of bulk Si. It can be noticed that all the as-grown samples have a decreasing lattice spacing with increasing C concentration. The d_{400} of pure Ge thin film shows a higher value than the relaxed bulk Ge, indicating that there is some epitaxial strain remaining in the pure Ge film. It is estimated from this d ratio that ~97% (of the total 4%) mismatch strain has been accommodated. For the Ge–C films with nominal $C<2$ at. %, a reduction in the d_{400} values (towards the bulk Ge value) indicates that the strain is relaxed by substitutional C and/or more efficient generation of misfit defects. For films with even higher nominal C content, the d_{400} value reduces below that of bulk Ge value and is clear evidence for the existence of substitutional C. The lowest d ratio measured indicates that a maximum of ~1 at. % C has been substitutionally alloyed with Ge (assuming Vegard's law). It is possible that interstitial C may also change the d ratio.[16]

After the anneal, it is observed that while the samples with lower C (<3 at. %) content show a decrease in the d ratio, the higher C content (>~5 at. %) films show an increase in the d ratio relative to the as-grown values. Possible reasons for this difference will be discussed later in the article.

C. Transmission electron microscopy results

Plan-view and cross-section transmission electron microscopy have been performed on most of the thin film samples. Some results have been previously published.[14,15] Typically, the cross-sectional TEM images show that the films are of good epitaxial quality for most of the films studied. Figure 3(a) is a cross-sectional image of a pure Ge film on Si(100), showing a majority of the misfit defects localized near the interface, a few threading dislocations, and no planar defects. With increasing C concentration, in addition to the misfit defects near the interface, the planar defect (e.g., stacking faults and microtwins) density is increased, as seen from Figs. 3(b) and 3(c). Furthermore, the growth fronts change from being flat to microscopically rough with increasing C contents, which is consistent with our RHEED observations.

Plan-view TEM images show that the pure Ge and Ge–C films on Si substrates are relaxed with short interfacial misfit dislocations as evidenced by the presence of moiré fringes and from weak-beam dark-field images as shown, for example, in Fig. 3(d).

After annealing, there is a major difference between the low carbon content (<5 at. %) films and the higher carbon content films. For lower carbon content films, the misfit dislocation density seems to have increased while the threading dislocation and the planar defect density seem to have decreased relative to the as-grown films as seen by comparing Fig. 3(a) with 4(a) and Fig. 3(b) with 4(b). For higher C films, the most significant change appears to have occurred at the interface as seen by comparing Fig. 3(c) to 4(c). A 2 to 3-nm-thick, bright interfacial layer has developed where the lattice fringes are not resolved and is likely to be amorphous. On the substrate side of the interfacial layer, a darker layer is also apparent. It is likely that the bright amorphous layer is C and/or Si rich (lower atomic mass leading to higher electron transmission), while the darker contrast on the substrate side is from Ge enrichment. The possible origins of the amorphous layer will be addressed in the next section.

Figure 5(a) is a cross-sectional TEM image of sample C, Ge–C thin film on Ge substrate. The image shows several interesting features. First, the growth front shows sharp {311} faceting. Second, within the thin film layer, dark lines of contrast making an angle consistent with {311} type planes is observed. This contrast is likely due to strain associated with C atoms that appear to have preferentially segregated to {311} planes. Third, unlike growth on Si substrates, there are no signs of misfit or planar defects. The {311} faceting and roughening is consistent with the RHEED patterns observed for this sample. The plan-view image of this sample, Fig. 5(b), shows no moiré fringes but some strain contrast possibly due to C clusters.

D. Raman spectroscopy studies

Raman spectra of $Si_{1-x}Ge_x$ alloys have been studied in detail both experimentally[17–21] and theoretically.[19,22–25] These spectra show lines near 300, 400, and 500 cm^{-1}, that correspond, respectively, to the Ge–Ge, Ge–Si, and Si–Si local vibrational modes. The frequencies of these modes in free-standing alloys shift in systematic ways with alloy composition according to the combined effects of mass disorder and microscopic strain.[23] Similar effects are seen in $Si_{1-x}C_x$ and Si-rich $Si_{1-x-y}Ge_xC_y$ alloys, where the presence of a

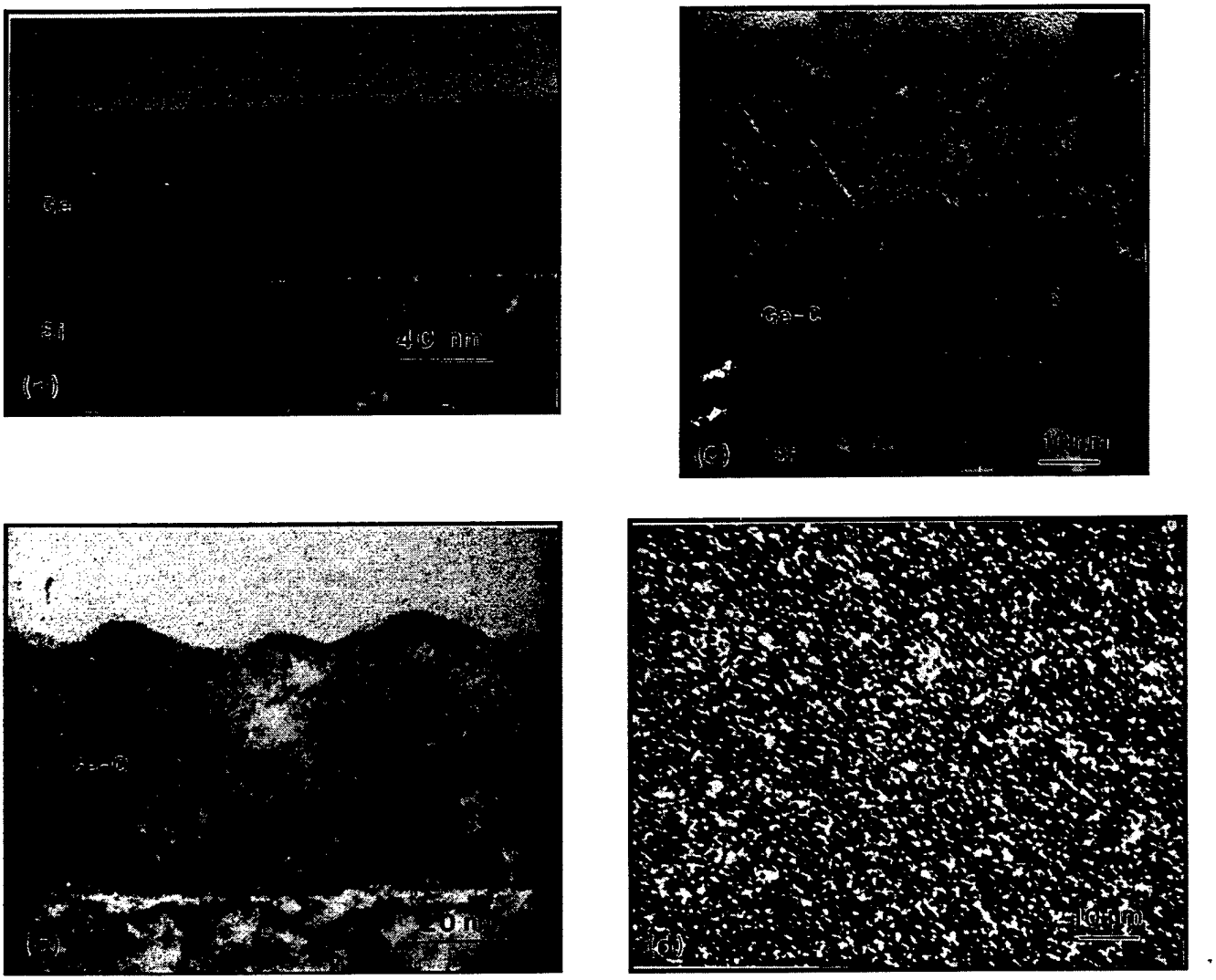

FIG. 3. (a) XTEM of Ge/Si, showing mostly relaxed film with some misfit dislocations at the interface, (b) XTEM of as-grown Ge–C (C=5%) film, showing planar defects in the film, (c) XTEM of as-grown Ge–C (C=10%) film with even larger planar defect density and some polycrystals developing, and (d) Plan-view of TEM (weak beam, dark field) of Ge–C (C=5%) film showing short misfit interfacial dislocations, similar to pure Ge on Si.

small amount (~1%) of substitutional C in the lattice is manifested by the appearance of an additional line near 600 cm^{-1} associated with the Si–C local mode.[7,23,26–28] In the $Ge_{1-x}C_x$ alloys of the present study, we see no clear evidence for Ge–C local mode to confirm the existence of substitutional C. This signal is possibly masked by a weak second order Ge peak that occurs near the frequency range of interest. There are, however, systematic C-induced changes in the band gap,[29] in the lattice constants and the optical properties[14] and similar changes in the Ge–Ge mode frequency, to be discussed in more detail here. We find that C induces a small negative shift of the Ge–Ge mode in the binary alloys, which we attribute to strain relaxation. As the C concentration increases, the Ge–Ge Raman mode develops a low-frequency shoulder, which we show is consistent with the Raman signature from amorphous Ge. In addition, an amorphous C peak is seen from all samples with nominal $C > \sim 2$ to 3 at. %.

The first question we wish to address in this section is the possibility that a Ge–C local mode can be seen in the Raman spectra. Meléndez–Lira *et al.*[28] suggest that a feature they observed near 560 cm^{-1} in $Si_{1-x-y}Ge_xC_y$ alloys could be assigned to a Ge–C mode or to a Si–C mode with two C atoms as second neighbors. This is indeed the frequency region in which one would expect to find the Ge–C mode. We see a similar feature in the Ge–C binary alloys, for which the possibility of a Si–C vibration is ruled out. However, as discussed below, this feature appears to coincide with a weak second-order Ge peak.

Figure 6 shows three spectra obtained under identical conditions from a Ge(100) wafer (lower curve), from a pure Ge epilayer on Si(100) (middle curve), and from a nominal $Ge_{0.93}C_{0.07}$ epilayer on Si(100). The Ge-wafer spectrum shows the strong Ge–Ge mode at 301.7 cm^{-1} and a number of weak second-order features, despite the fact that the polarization geometry has been chosen to allow first-order and suppress second-order scattering. The spectra from the films show these same lines plus the *c*-Si line at 521 cm^{-1} and the second-order Si band above 900 cm^{-1}. The region of interest is the valley between the second-order Ge peak at 575 cm^{-1}

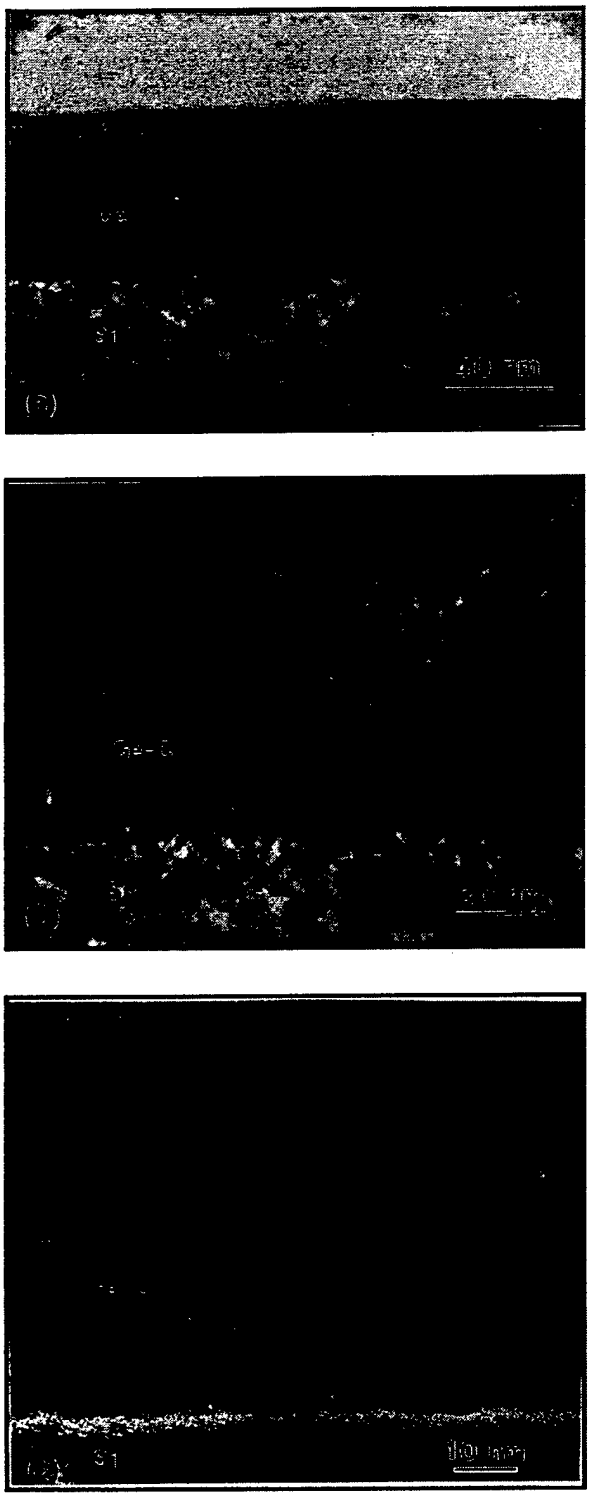

FIG. 4. (a) XTEM of Ge on Si after annealing showing significantly reduced threading defects, (b) XTEM of Ge–C (5% C) on Si after annealing, showing more misfit dislocations on the interface and less planar defects within the film, and (c) XTEM of Ge–C (10% C) after annealing. Note the white straight amorphous layer near the interface, possibly due to formation of a-C or silicon carbide.

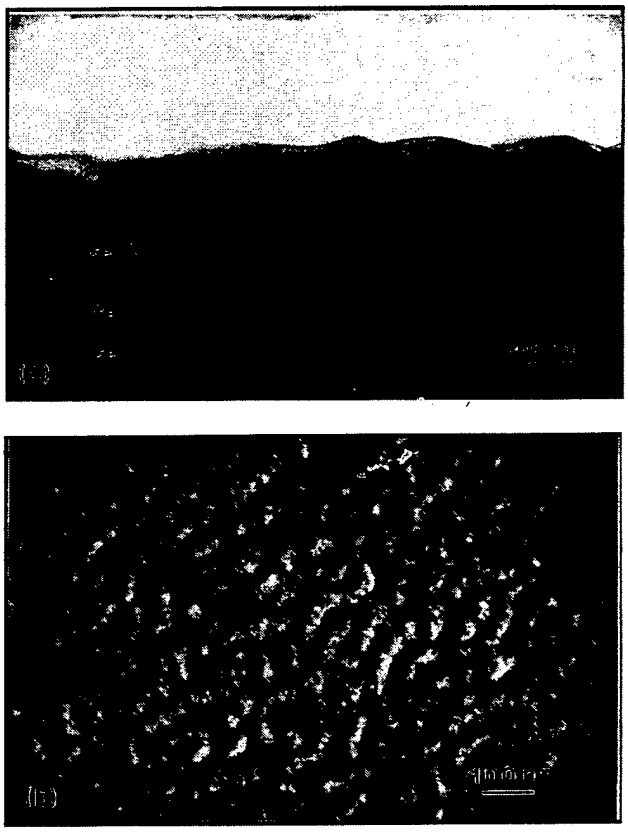

FIG. 5. (a) XTEM of Ge–C(5% C) on Ge. Note the strong (311) faceting and C clusters decorating {311} planes. (b) Plan-view of Ge–C(5% C) on Ge shows strong strain contrast but no moiré fringes.

and the c-Si peak. Note that this valley is less deep in the C-doped film than it is in the pure-Ge film, suggesting that there may be some extra intensity in this region due to the Ge–C local mode. However, the overlap from the wings of the Si peak and the second-order Ge peak make it impossible to extract a "peak" attributable to a Ge–C local mode. Furthermore there is extra intensity, probably fluorescence, in the entire spectrum from the C-doped film. In other words, there is no clear signature in the Raman spectra of such a local mode. With a shorter wavelength pump laser, which would not penetrate to the substrate, or with much thicker films, the interference from the Si peak could be eliminated, but the second-order Ge feature will always interfere.

The shift in the frequency of the Ge–Ge Raman mode produced by C doping is extremely small, typically less than 10%–20% of the linewidth, and less than the frequency interval between points in the spectra. In order to measure this shift accurately, it is imperative that we use an analytical lineshape function that gives a good fit to the experimental data. The peak frequency will then correspond to the maximum value of this function. We have found that simple Lorentzians or Gaussians do not give a good fit to the experimental lineshapes, even for the pure Ge films. Moreover, with C added, the line becomes asymmetric. We have thus chosen to use Pearson-type lineshape functions to fit these lines.[30] For the pure Ge films, we use a symmetrical Pearson VII distribution:

$$f(\omega)=\alpha_0\left[1+4\left(\frac{\omega-\alpha_1}{\alpha_2}\right)^2(2^{1/\alpha_3}-1)\right]^{-\alpha_3}, \tag{1}$$

where α_0 is the amplitude, α_1 is the peak frequency, α_2 is the width, and α_3 is a shape parameter. When $\alpha_3=1$, the

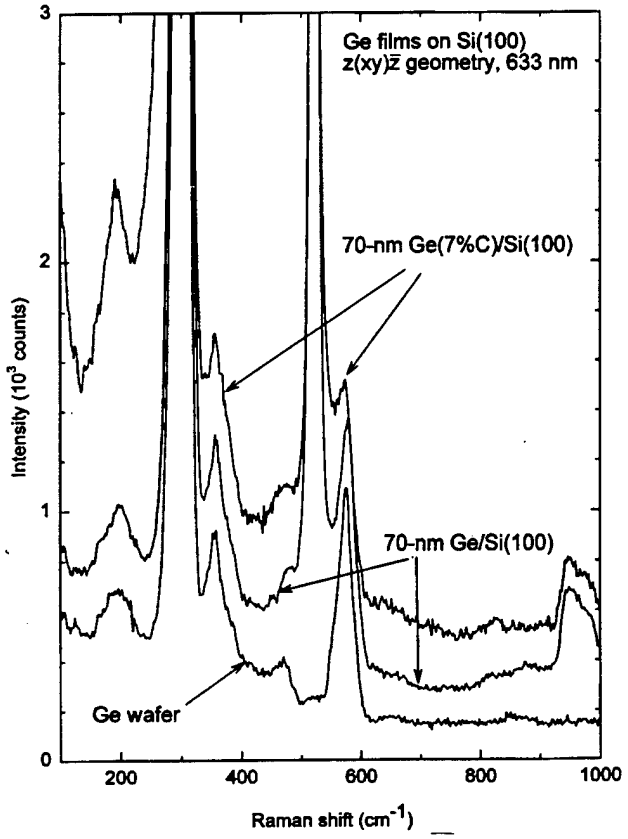

FIG. 6. Polarized Raman spectra from an oriented wafer of Ge (100) (lower curve), a pure Ge film on Si(100) (middle curve), and a Ge–C(7%) film on Si(100) (upper curve).

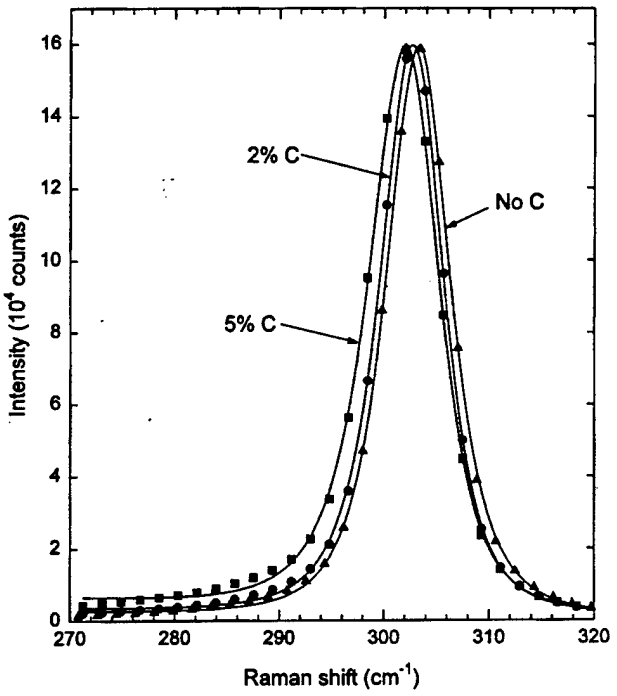

FIG. 7. Data points are polarized Raman spectra, as in Fig. 6, of the Ge–Ge mode, after subtracting a linear background, for three epitaxial films grown on Si(100). The solid lines are least-squares fits to Eq. (1) for the pure Ge film and to Eq. (2) for the Ge–C films. The spectra have been scaled slightly to have the same peak amplitude.

function is a Lorentzian, and as α_3 becomes large the shape tends toward a Gaussian. This lineshape is widely used as a simple analytical approximation to the better-known Voight function.

For the C-doped films, we use an asymmetric Pearson IV lineshape:

$$f(\omega)=\alpha_0(1+x^2)^{-\alpha_3}\exp\left\{-\alpha_4\left[(\tan^{-1}x)+\tan^{-1}\left(\frac{\alpha_4}{2\alpha_3}\right)\right]\right\} \tag{2}$$

with

$$x=\frac{\omega-\alpha_1-\alpha_2\alpha_4/2\alpha_3}{\alpha_2},$$

where α_0 is the amplitude, α_1 is the peak frequency, α_2 is a width, and α_3 and α_4 are shape parameters. The asymmetry is determined by the sign of α_4, a positive value gives a low-frequency tail, a negative value a high-frequency tail.

Examples of our spectra along with fits to Eqs. (1) and (2) are shown in Fig. 7. The data points here are the raw spectra from which a linear background has been subtracted. For plotting purposes, the data for two of the plots have then been scaled slightly to yield the same peak intensity as the third. The solid lines in this figure are least-squares fits to the Pearson functions given above. Note that there is a small negative shift of the peak frequency with increasing C and that there is a substantial tail on the low-frequency side of the 5% C curve. A summary of all the frequency-shift data is given in Fig. 8. The error bars in this figure are 2.5 times the standard deviation of c-Si peak frequency measured at the same time from the same spectra. We consider these error bars to be conservative estimates of the experimental uncer-

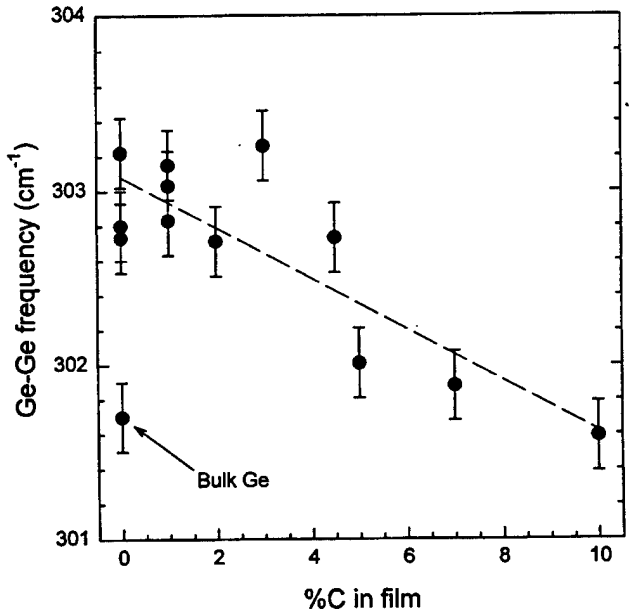

FIG. 8. Plot of the Ge–Ge frequency, determined by fits as in Fig. 7, as a function of C concentration in the films. The lower left point is for a Ge wafer. The dashed line is a linear least-squares fit to show the trend.

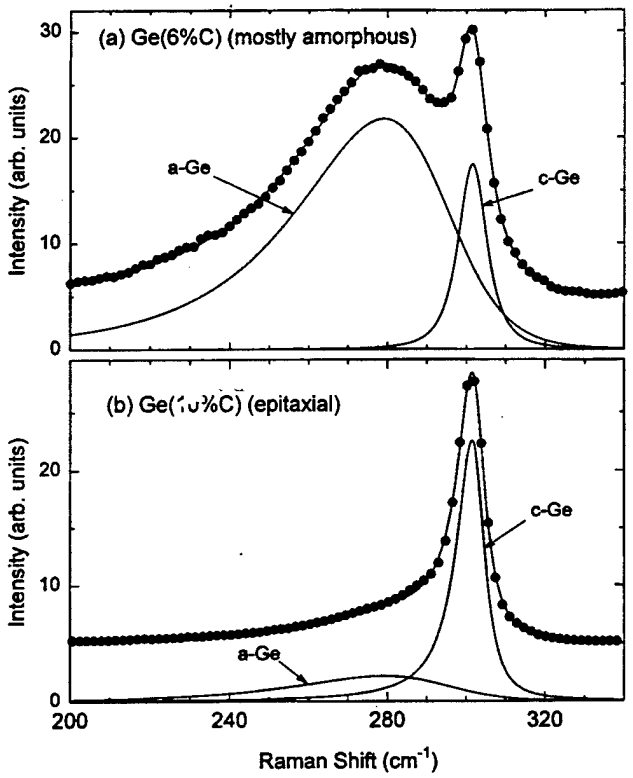

FIG. 9. Raman spectra after linear background substraction of amorphous (a) and crystalline (b) Ge–C films. The data points and the resultant fits (solid curves) are shifted up by one vertical tick mark for clarity. The decomposition of the spectrum in (a) into two peaks, one for a-Ge the other for c-Ge shown below the data, is done with a full least-squares minimization. The a-Ge lineshape determined in (a) is then constrained to be the same in (b).

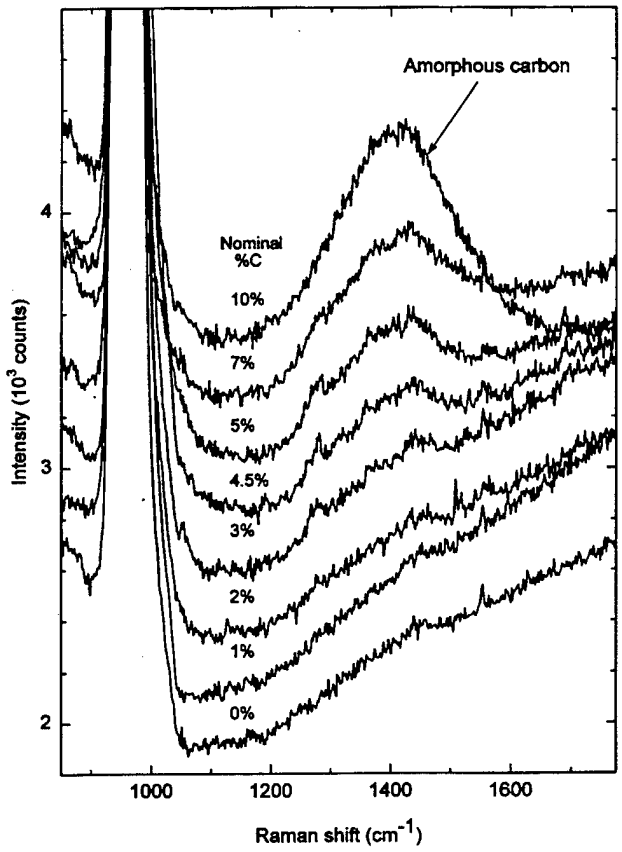

FIG. 10. Unpolarized Raman spectra from Ge–C films showing the broad band from amorphous C at the highest concentrations. The spectra have been systematically shifted by a few hundred counts in order to make a nearly evenly spaced stacked plot.

tainty, since the Ge peak is actually bigger than the c-Si peak. Although there is considerable scatter in the points, the trend toward lower frequency with increasing C is convincing.

There are three effects contributing to the shifts shown in Fig. 8: mass disorder, microscopic strain, and epitaxial strain due to the lattice mismatch between film and substrate. The last of these can be calculated from measurements of the film lattice constants and the known deformation parameters for the phonon. Our x-ray data indicate that the pure Ge films have positive strain in the direction normal to the surface, $\epsilon_{zz}=2.4\times10^{-3}$, and a corresponding negative in-plane strain, $\epsilon_{xx}=-(C_{11}/2C_{12})\epsilon_{zz}=-3.2\times10^{-3}$, where the C_{ij} are the Ge elastic constants. This biaxial strain will split the triply degenerate zone-centered Raman phonon into a singlet and a doublet. Only the singlet will be observed in our scattering geometry, and its dependence on the strain is given by Refs. 23 and 31:

$$\omega=\omega_0\left[1-\gamma(2\epsilon_{xx}+\epsilon_{zz})-\frac{p-q}{3\omega_0^2}(\epsilon_{xx}-\epsilon_{zz})\right], \tag{3}$$

where ω_0 is the frequency in an unstrained lattice, γ is the Grüneisen parameter, and $(p-q)/3\omega_0^2$ is a coefficient describing the strain dependence of the internal force field. Using the values $\gamma=0.89$ and $(p-q)/3\omega_0^2=0.15$, measured by Cerdeira *et al.*,[31] we calculate a shift of $+1.3\ \mathrm{cm}^{-1}$ for the epitaxial film. This value agrees well with our measured value of $1.2\pm0.2\ \mathrm{cm}^{-1}$ from the data in Fig. 8.

As the C concentration increases, the Ge lattice parameter normal to the surface decreases, which has the tendency to relax the strain (island formation is also relaxing the strain, but it is difficult to separate the two effects). The strain relaxation shifts the peak towards the frequency for bulk Ge. Based on the x-ray diffraction data, we notice that the strain is already relaxed (i.e., bulk Ge lattice parameter is reached) for films with more than ~2 at. % nominal C. However, the Raman data still show a positive shift compared to bulk Ge. It is therefore likely that this shift is a net result of the influence of C-induced microscopic strain and mass disorder.

A third interesting feature observed in our Raman data is that at the highest C concentrations a broad shoulder near $280\ \mathrm{cm}^{-1}$ is observed that cannot be fit with a single Pearson IV lineshape. We accidentally discovered an extreme example of this shoulder in an attempt to grow a 6 at. % C film on a substrate from which the oxide was not completely removed. The result was a nearly amorphous film, as indicated by x-ray analysis. The Raman spectrum from this film is shown in Fig. 9(a). This spectrum is composed of two peaks, a broad highly asymmetric band centered near $280\ \mathrm{cm}^{-1}$ and a narrow peak at $301.6\ \mathrm{cm}^{-1}$. The broad band is the signature for amorphous Ge,[32,33] and the narrow peak

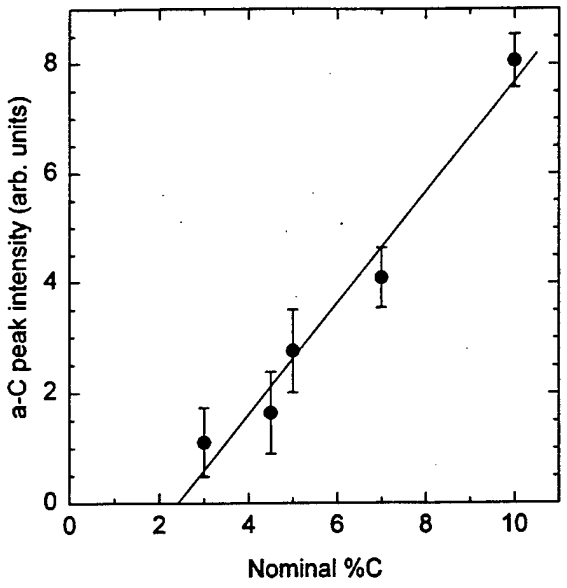

FIG. 11. Amorphous C Raman peak intensity as a function of C concentration as described in the text. The straight line is a linear least-squares fit.

is from Ge crystallites embedded in the mostly amorphous film. The frequency of the narrow peak matches well with that for fully relaxed crystalline Ge.

The spectrum in Fig. 9(b) is from an epitaxial $Ge_{0.9}C_{0.1}$ film. It is fit by using the same lineshape for the broad band from Fig. 9(a), in which only the amplitude is varied, along with the usual Pearson IV lineshape for the narrow peak. The fit is convincing. The broad shoulder is completely accounted for by allowing for a small contribution from the a-Ge lineshape. We conclude that the high C films have an increasing fraction of amorphous Ge.

Raman measurements were also made in the 800–1800 cm^{-1} range to explore the possibility of C-related vibrational modes. Figure 10 shows a series of spectra for various Ge–C alloys. The signature of amorphous C, a broad band peaking near 1400 cm^{-1} is clearly seen for the higher C films.[34] The 10 at. % C film was fitted to get the lineshape, which was then constrained to obtain the peak strength for the rest of the plots, as shown in Fig. 11. A straight line fit to the data gives an intercept of 2.4% below which no a-C peak is present.

Annealing produces a major change in the C–C region of the spectrum, as shown in Fig. 12. The annealed films have a double-peak structure characteristic of graphitic carbon. There is a fairly broad line near 1330 cm^{-1}, corresponding to the disorder-induced zone-boundary phonon from graphite and a narrower line at 1598 cm^{-1}, corresponding to the zone-center E_{2g} mode. This material is also called glassy carbon or microcrystalline graphite.[35,36] The graphitic C bands are much stronger than the a-C band in the unannealed samples, but that is probably due to the resonance effect owing to a strong optical absorption in graphite.

IV. DISCUSSION

A. Incorporation of C in $Ge_{1-x}C_x$ films

Our experimental results are consistent with the following model. When the nominal C concentration is less than

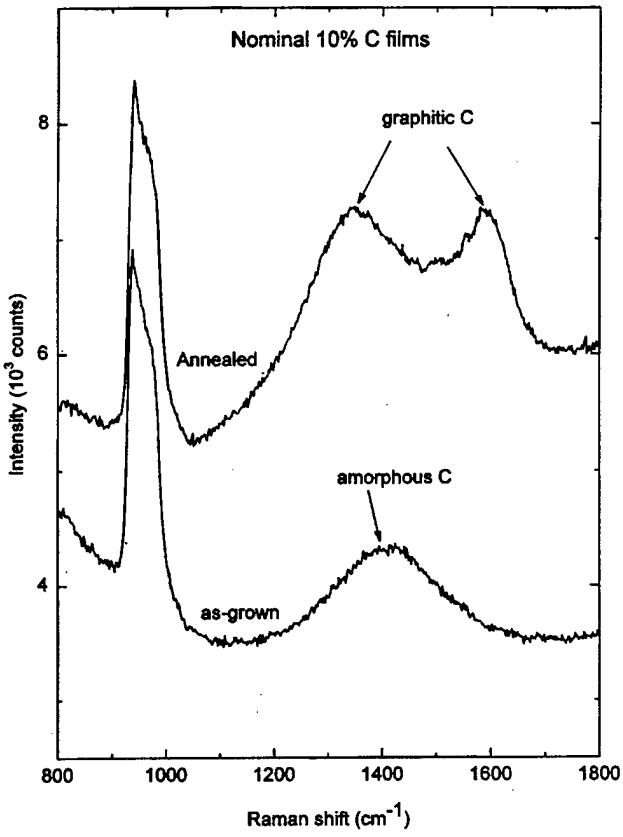

FIG. 12. Effect of annealing on a nominal Ge–C (10%) film. Note the change in the a-C peak to a graphitic C double-peaked structure.

~2 to 3 at. %, the deposited C is predominantly dispersed either substitutionally and/or interstitially. This results in the same growth mode as pure Ge, aside from the fact that the films have a lower lattice parameter due to substitutional incorporation of C. When the increase in the C flux leads to an increase in the nominal C>~3 at. %, not only does more C go into Ge substitutionally (as indicated by the x-ray data), but also the growth mode changes from 2D to 3D islanding/facet formation after initial few MLs of Ge–C codeposition. While there may be a marginal increase in the substitutional fraction due to an increase in the C growth rate,[8] it is suggested, based on correlation of the a-C observed by Raman with the RHEED and TEM results, that the excess a-C is responsible for the change in growth mode from 2D layer to 3D island growth (discussed in Sec. IV B). The formation of planar defects in the $Ge_{1-x}C_x$ films with nominal C>3 at. % is likely to be a consequence of island coalescence in the presence of strain (In the absence of significant strain, e.g., Ge–C on Ge, planar defects do not seem to form). Consequently, the tendency for island formation increases with increased nominal C concentration leading to an increased density of planar defects.

In the particular case of the $Ge_{1-x}C_x$ ($x=5$ at. %) films grown on Ge substrates, the epitaxial mismatch strain is unlikely to be very high, based on the fact that no extra Ge–C peak can be detected in the x-ray 2θ scans. This is also consistent with our observation that no misfit induced defects are found in TEM studies. In this case, the excess C not only

changes the growth mode from layer to 3D islands, but also the excess C is forced to precipitate/segregate along {311} planes, as seen in Fig. 5(a). One likely reason as to why the {311} planes are specifically decorated in $Ge_{1-x}C_x$ films grown on Ge may be related to a lower surface energy of Ge–C {311} compared to Ge–C {100} planes, as calculated for Si surfaces.[37,38] In the case of $Ge_{1-x}C_x$ films on Si, the tendency to facet along {311} is less pronounced possibly due to kinetic constraints (growth of $Ge_{0.95}C_{0.05}$ on Si at 550 °C leads to strong {311} faceting). The lack of decoration of {311} facets in $Ge_{1-x}C_x$/Si may be due to the fact that some of the C may be incorporated at the high density of defect (planar and misfit) sites and from epitaxial strain effects.

B. The driving force for 2D to 3D transition

It is well known that pure Ge grown on Si follows the layer plus island or the Stranski–Krastanow growth mode. This is because island formation relieves the strain energy at the expense of increased surface area. However, by maintaining a sufficiently low substrate temperature (e.g., 200 °C), the reduced surface diffusion suppresses island formation, as confirmed by our RHEED and TEM observations. In our studies of Ge–C alloys, the presence of C>3 at. % leads to 3D island formation even at this low substrate temperature (200 °C). The possible reasons[14] for this behavior could be (i) increased strain-induced surface diffusion in the presence of C,[39] (ii) changes in surface energetics/wetting behavior due to C, or (iii) heterogeneous nucleation at C clusters.[40]

We rule out nucleation at C clusters as a possibility because Ge growth on a rough Ge–C surface rapidly becomes planar at this growth temperature. While increased surface diffusion is a possibility, the islanding tendency is not due to strain alone as evident from the fact that Ge–C grown on Ge tends to grow 3D. The most likely reason appears to be a change in surface energies of the Ge–C film relative to Si and Ge, leading to either changes in the wetting behavior or an increased tendency to lower their surface energy by forming specific crystallographic facets, e.g., {311}.

The wetting behavior may be explained on the basis of the following qualitative argument. It is proposed that the surface energy of Ge–C is larger than that of Ge and is a linear function of C concentration (It is assumed that the interfacial energies involved are all the same). The surface energy of pure Si is known to be larger than that of pure Ge and explains why Ge wets Si. On that basis, it can be understood that a Ge–C film with low C concentration would have a surface energy lower than that of Si and is likely to grow in a layer mode. Ge–C films with higher C concentration and whose surface energy is larger than that of Si may grow in an island mode. In our experiments, this cross-over appears at a C concentration of about 3 at. %. This C rich surface subsequently lowers its energy by faceting along {311} planes. This model explains the observed morphology in the experiments involving the growth of Ge–C on Si, Ge–C on Ge, and Ge on Ge–C films at 200 °C. The only apparent exception is the growth of Si on $Ge_{0.95}C_{0.05}$ where 3D growth was observed after 20 nm of Si deposition, even though our model would predict 2D growth. It is however conceivable that by forming facets, the Ge–C may have reduced its surface energy to a value below that of Si. An alternative explanation is the lack of sufficient kinetics for Si to smooth out the roughness on a Ge–C (100) surface.

C. Effect of annealing

Annealing at 750 °C causes measurable changes in the microstructure and composition of the Ge–C alloys. From the x-ray data (Fig. 2) for the annealed samples, it can be noted that for pure Ge and low C(<3 at. %) concentration alloys, annealing leads to a marginal reduction in the lattice parameter below that of bulk Ge (i.e., the dashed line). One cause for the decrease in lattice parameter could be that the amount of substitutional C may have increased. In addition, Si interdiffusion into the films during the anneal may also contribute to this effect. The presence of ~2–4 at. % Si has been measured in our annealed samples by Raman spectroscopy.[41] The postannealed samples also appear to have a higher density of interfacial misfit dislocations as seen by comparison of Figs. 3 and 4, while the density of planar defects and threading defects seems to have decreased significantly. All of these effects can contribute to the decrease of the lattice parameter relative to the as-grown films.

For higher C films (>5 at. %), the x-ray data indicate that the lattice parameter increases after the anneal. A likely explanation is that a significant amount of C has been ejected out of the substitutional sites, and that this effect outweighs the reduction in lattice parameter due to interdiffused Si. A second microstructural feature of significance is the amorphous layer formed at the Ge–C/Si interface. This layer appears only after the anneal and seems to be rich in low atomic number elements (e.g., C) as deduced from the TEM contrast. Since the diffusivity of Si and Ge is likely to be larger than C, and a driving force exists to form the stable compound SiC, a C-rich Si–C amorphous layer may have formed at the interface. Further work is needed to characterize the composition and understand the formation of this layer.

The incorporation of C and the growth mechanism of Ge–C alloys on Si at low temperature can be summarized as follows. We start with the assumption that there is a limited "substitutional solubility" and "interstitial solubility" of C in Ge in the thin film state. This solubility depends on the growth conditions (e.g., temperature, flux, and the strain). Since most of our films were on Si substrates and grown at 200 °C, the growth temperature and the epitaxial strain are maintained nearly constant. Under these conditions, the equilibrium solubilities are almost constant (depending only on the C flux). At low nominal C content, the deposited C is distributed both substitutionally and interstitially and the growth front is planar. Beyond the solubility limit, the excess C exists in the form of *a*-C on the surface (i.e., at the growth front) and alters the growth mode from 2D layer to 3D growth. This transition occurs about 3 at. % in our studies. For C contents larger than ~5 at. %, the coalescence of the 3D islands (in the presence of strain) leads to the formation of a high concentration of planar defects (e.g., stacking faults and microtwins) as seen from the cross-sectional TEM im-

ages. For even higher C contents, the presence of a high concentration of a-C degrades the epitaxial quality of the film.

ACKNOWLEDGMENTS

We thank Joe Mclaughlin for help with TEM sample preparation, Barry Wilkens (ASU) for RBS analysis, and Ed Laitila for technical help. Financial support for this research has been provided by the Office of Naval Research (N00014-96-1-0793).

[1] J. C. Bean, Proc. IEEE **80**, 571 (1992).
[2] R. A. Soref, Proc. IEEE **81**, 1687 (1993).
[3] A. R. Powell, F. K. LeGoues, and S. S. Iyer, Appl. Phys. Lett. **64**, 324 (1994).
[4] J. L. Regolini, S. Bodnar, J. C. Oberlin, F. Ferrieu, M. Gauneau, B. Lambert, and P. Boucaud, J. Vac. Sci. Technol. A **12**, 1015 (1994).
[5] M. Todd, P. Matsunaga, J. Kouvetakis, D. Chandrasekhar, and D. J. Smith, Appl. Phys. Lett. **67**, 1247 (1995).
[6] B. Dietrich, H. J. Osten, H. Rücker, M. Methfessel, and P. Zaumseil, Phys. Rev. B **49**, 17 185 (1994).
[7] K. Eberl, S. S. Iyer, S. Zollner, J. C. Tsang, and F. K. LeGoues, Appl. Phys. Lett. **60**, 3033 (1992).
[8] H. J. Osten, M. Kim, K. Pressel, and P. Zaumseil, J. Appl. Phys. **80**, 6711 (1996).
[9] J. Mi, P. Warren, M. Gailhanou, J.-D. Ganiere, M. Dutoit, P.-H. Jouneau, and R. Houriet, J. Vac. Sci. Technol. B **14**, 1660 (1996).
[10] H. J. Osten, Mater. Sci. Eng. B **36**, 268 (1996).
[11] H. J. Osten, E. Bugiel, and P. Zaumseil, J. Cryst. Growth **142**, 322 (1994).
[12] J. Kolodzey, P. A. O'Neil, S. Zhang, B. A. Orner, K. Roe, K. M. Unruh, C. P. Swann, M. M. Waite, and S. Ismat Shah, Appl. Phys. Lett. **67**, 1865 (1995).
[13] M. Todd, J. Kouvetakis, and D. J. Smith, Appl. Phys. Lett. **68**, 2047 (1996).
[14] M. Krishnamurthy, B.-K. Yang, and W. H. Weber, Appl. Phys. Lett. **69**, 2572 (1996).
[15] B.-K. Yang, J. D. Weil, and M. Krishnamurthy, Mater. Res. Soc. Symp. Proc. **440** (to be published).
[16] W. Windl, J. D. Kress, A. F. Voter, J. Menéndez, and O. F. Sankey, Mater. Res. Soc. Symp. Proc. **469** (to be published).
[17] M. A. Renucci, J. B. Renucci, and M. Cardona, in *Proceedings of the Conference on Light Scattering in Solids*, edited by M. Balkanski (Flamarion, Paris, 1971), p. 326.
[18] J. Menéndez, A. Pinczuk, J. Bevk, and J. P. Mannaerts, J. Vac. Sci. Technol. B **6**, 1306 (1988).
[19] M. I. Alonso and K. Winer, Phys. Rev. B **39**, 10 056 (1989).
[20] D. J. Lockwood and J.-M. Baribeau, Phys. Rev. B **45**, 8565 (1992).
[21] J. C. Tsang, P. M. Mooney, F. Dacol, and J. O. Chu, J. Appl. Phys. **75**, 8098 (1994).
[22] S. Gironcoli, Phys. Rev. B **46**, 2412 (1992).
[23] H. Rücker and M. Methfessel, Phys. Rev. B **52**, 11 059 (1995).
[24] Z. Sui and I. P. Herman, Phys. Rev. B **48**, 17 938 (1993).
[25] J. Zi, K. Zhang, and X. Xie, Phys. Rev. B **45**, 9447 (1992).
[26] J. Menéndez, P. Gopalan, G. S. Spencer, N. Cave, and J. W. Strane, Appl. Phys. Lett. **66**, 1160 (1995).
[27] H. Rücker, M. Methfessel, B. Dietrich, K. Pressel, and H. J. Osten, Phys. Rev. B **53**, 1302 (1996).
[28] M. Meléndez-Lira, J. Menéndez, W. Windl, O. F. Sankey, G. S. Spencer, S. Sego, R. B. Culbertson, A. E. Bair, and T. L. Alford, Phys. Rev. B **54**, 12 866 (1996).
[29] B. A. Orner, A. Khan, D. Hits, F. Chen, K. Roe, J. Pickett, X. Shao, R. G. Wilson, P. R. Berger, and J. Kolodzey, J. Electron. Mater. **25**, 297 (1996).
[30] J. K. Ord, *Families of Frequency Distributions* (Hafner, New York, 1972), p. 6.
[31] F. Cerdeira, C. J. Buchenauer, F. H. Pollak, and M. Cardona, Phys. Rev. B **5**, 580 (1972).
[32] M. Wihl, M. Cardona, and J. Tauc, J. Non-Cryst. Solids **8–10**, 172 (1972).
[33] M. H. Brodsky, in "Light Scattering in Solids I," *Topics in Applied Physics*, Vol. 8, edited by M. Cardona (Springer, Berlin, 1983), p. 205.
[34] J. E. Smith, M. H. Brodsky, B. L. Crowder, and M. I. Nathan, J. Non-Cryst. Solids **8–10**, 179 (1972).
[35] M. Yoshikawa, N. Nagai, M. Matsuki, H. Fukuda, G. Katagiri, H. Ishida, A. Ishitani, and I. Nagai, Phys. Rev. B **46**, 7169 (1992).
[36] J. Wagner, M. Ramsteiner, Ch. Wild, and P. Koidl, Phys. Rev. B **40**, 1817 (1989).
[37] D. M. Bird, L. J. Clarke, R. D. King-Smith, M. C. Payne, I. Stich, and A. P. Sutton, Phys. Rev. Lett. **69**, 3785 (1992).
[38] Y.-N. Yang and D. Williams, J. Vac. Sci. Technol. A **8**, 2481 (1990).
[39] J. Tersoff, Phys. Rev. Lett. **74**, 5080 (1995).
[40] P. O. Pettersson, C. C. Ahn, T. C. Mcgill, E. T. Croke, and A. T. Hunter, J. Vac. Sci. Technol. B **14**, 3030 (1996).
[41] B.-K. Yang, M. Krishnamurthy, and W. H. Weber (unpublished).

Low-temperature epitaxial growth of Ge-rich Ge–Si–C alloys: Microstructure, Raman studies, and optical properties

B.-K. Yang and M. Krishnamurthy[a)]
Department of Metallurgical and Materials Engineering, Michigan Technological University, Houghton, Michigan 49931

W. H. Weber
Physics Department, Ford Motor Company, Dearborn, Michigan 48121-2053

(Received 19 November 1997; accepted for publication 6 May 1998)

Low-temperature (~200 °C) molecular beam epitaxy of Ge-rich $Ge_{1-x-y}Si_yC_x$ alloys grown on Si(100) have been investigated by *in situ* reflection high-energy electron diffraction, *ex situ* x-ray diffraction, transmission electron microscopy, Raman scattering, and ellipsometry. The Si contents were either ~20 or ~40 at % and the C concentrations were nominally varied from zero up to ~8 at %. Selected samples were annealed in an Ar ambient at 750 °C to evaluate the stability of the thin films. With increasing C concentration, the epitaxial growth mode changes from two-dimensional (2D) layer growth to 3D island growth. Under the growth conditions studied, the GeSiC films have a tendency to form planar defects, whose density increases with increasing C and Si concentrations. The x-ray diffraction data show that the lattice parameter decreases with increasing C concentration. It is estimated that a maximum of ~2–3 at % C is substitutionally incorporated into these films. Raman spectra of the alloy films show that the effects of C on the strong Ge–Ge and Ge–Si local modes are far less than the effects due to Si. We are unable to observe any systematic change in the Ge–Ge mode, whereas the Ge–Si mode appears to shift to lower frequency with the small addition of C. $Ge_{1-x-y}Si_yC_x$ films formed by annealing $Ge_{1-x}C_x$ films on Si are also discussed. Spectroscopic ellipsometry determinations of the film's optical constants show that the primary effect of C is to reduce the strength of the E_1 critical point feature. © *1998 American Institute of Physics.* [S0021-8979(98)02316-0]

I. INTRODUCTION

SiGe alloys have been extensively studied in order to exploit the promise of band-gap engineering on silicon.[1] In the past few years, alloys of group IV elements including C, Si, Ge, and Sn have been actively investigated for use in heterojunction devices compatible with current Si integrated circuit technology.[2,3] There has been a particularly strong interest in SiGe alloys containing carbon. The main reason is that (assuming Vegard's law) an approximately 9:1 Ge to C ratio is expected to lattice match SiGeC alloys to Si, circumventing critical thickness limitations inherent in SiGe technology. Furthermore, C in the SiGe lattice makes it possible to use both alloy concentration and strain as a variable for band-gap engineering. However, several obstacles must be overcome. First, C is relatively insoluble in both Ge and Si, unlike the completely miscible SiGe system. Second, the formation of various forms of SiC is thermodynamically favored at higher growth temperatures.

Despite these problems, low concentrations of C in Si–Ge–C have been successfully incorporated using a variety of techniques including chemical vapor deposition (CVD),[4–8] molecular beam epitaxy (MBE),[9–11] and solid phase epitaxy.[12] Those thin film alloys were typically grown at temperatures between 400 and 650 °C, with a Ge content of 20 at %,[3] 30 at %,[5] 40 at %,[6] or even less, with substitutional C levels up to ~2–3 at %,[6,10] with little emphasis on the Ge-rich ternary system, except for Ref. 10. For a review of the growth and properties of SiGeC alloys, see Ref. 13.

We have recently reported[14,15] on the microstructural evolution and optical properties of the $Ge_{1-x}C_x$ alloys ($x<0.1$) grown at ~200 °C. In this article we present the effect of adding Si to $Ge_{1-x}C_x$ alloys grown on Si(100) substrates at ~200 °C. The reasons for using such a low temperature (reduced kinetics) are to suppress phase separation and to prevent SiC precipitation. In addition, it has also been observed in the Si–C system that a reduction in growth temperature leads to an increase in the substitutional-to-interstitial carbon ratio.[16] Our selection of 200 °C is based on the fact that it is an estimated lower limit for good epitaxial growth. The films were characterized *in situ* by reflection high-energy electron diffraction (RHEED) and *ex situ* by transmission electron microscopy (TEM) and x-ray diffraction (XRD). Optical characterization was performed using Raman spectroscopy and spectroscopic ellipsometry (SE).

II. EXPERIMENTS

The $Ge_{1-x-y}Si_xC_y$ films were grown in a Riber 32 MBE system with a base pressure of better than 5×10^{-10} Torr. Si(100) substrates were chemically cleaned and oxidized by boiling in a H_2O_2:H_2SO_4 mixture. After the sample had been degassed in the MBE at ~200 °C overnight, the oxide was desorbed by heating to just below 900 °C for about 15 min

a)Electronic mail: mohan@mtu.edu

 © 1998 American Institute of Physics

and then the sample temperature was quickly dropped to ~200 °C. Sharp (2×1) diffraction spots indicative of a clean surface were typically observed in RHEED. In all cases, in order to produce a better quality surface, a couple of monolayers of Ge were deposited on the sample surface at 200 °C soon after the above oxide desorption, followed by reheating to ~800 °C for complete oxide desorption. After the above Ge-assisted oxide desorption, the RHEED showed a sharper (2×1) reconstruction pattern indicating a better quality surface. Germanium was deposited from a previously calibrated pyrolytic boron nitride Knudsen source at ~0.5 or 1 nm/min. The C was deposited from a rod-fed electron-beam source, and the flux was varied to obtain various C concentrations. Si was also deposited from a rod-fed electron-beam source whose flux was kept constant at ~0.3 nm/min. Rutherford backscattering spectrometry (RBS) (including C resonance) was used to estimate the C and Si concentrations. A typical experiment consisted of the following steps. After the sample had stabilized at ~200 °C, the Ge shutter was first opened followed by the Si and C shutters after a 10–30 s delay. The nominal thickness for most of films varied from 30 to 70 nm. Two groups of ternary alloys have been studied, namely (i) type A: high Ge content alloys, with ~75% Ge, the balance being Si about 20% and C varying; (ii) type B: low Ge content alloys with ~55% Ge, the balance being Si about ~40% and C varying.

The Raman measurements were done using a Renishaw 1000 Raman microscope with 633 nm excitation. The experimental apparatus and the line shape fitting procedure are described in more detail elsewhere.[15] The spectroscopic ellipsometry data were recorded with a variable-angle, automated ellipsometer made by J. A. Woollam Co. Optical constants of the films were obtained by fitting to an expansion of ϵ as a sum of Lorentz oscillators representing the various critical points in the optical response of Si–Ge alloys. The position, strength, and width of all oscillators in the 1–5 eV range were optimized as were the film and native oxide thicknesses.

III. RESULTS

A. Reflection high-energy electron diffraction (RHEED) studies

The RHEED patterns of $Ge_{0.8}Si_{0.2}$, $Ge_{0.6}Si_{0.4}$ and $Ge_{0.78}Si_{0.2}C_{0.02}$ alloy thin films were streaky (2×1) patterns that remained almost unchanged throughout the growth. On addition of more C (>3–4 at %) the layers show initial layer growth followed by 3D island formation. For even higher C contents (>6 at %) the patterns changed quickly from (2×1) streaks to 3D transmission spots, eventually forming extra twinning-related spots at the end of the growth. The C-dependent changes in RHEED patterns associated with the low-temperature growth of Ge-rich GeSiC alloys are similar to those observed for low-temperature Ge–C alloys grown on Si.[14,15]

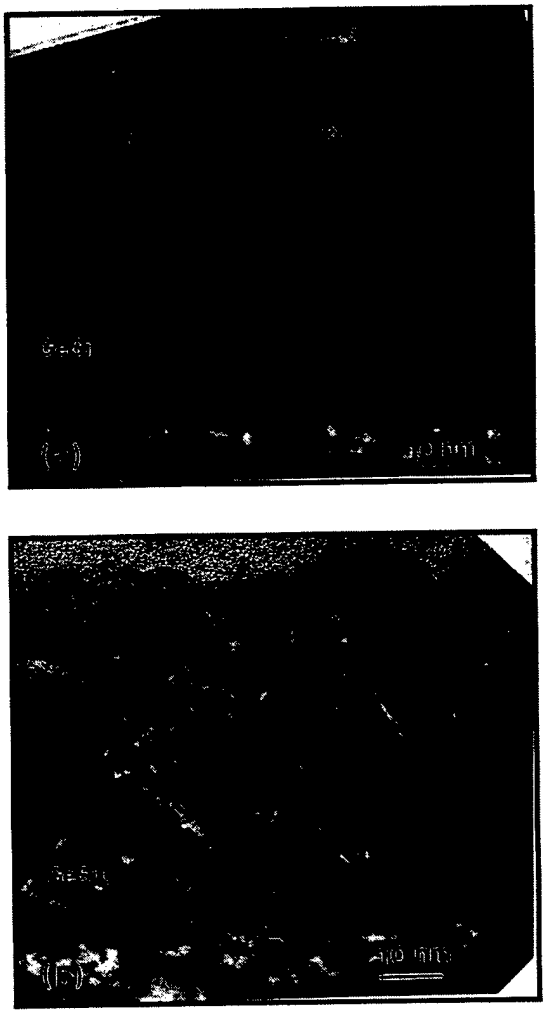

FIG. 1. XTEM images of (a) $Ge_{0.8}Si_{0.2}$ film, showing smooth growth front and some misfit defects at the interface, and (b) $Ge_{0.76}Si_{0.2}C_{0.04}$ film, showing rough growth front and planar defects in the film.

B. Transmission electron microscopy (TEM) characterization

The microstructural features of the high Ge and low Ge content GeSiC alloys are characterized by short interfacial misfit dislocations as observed in plan-view TEM. With increasing C content, an increasing density of planar defects is observed in cross-sectional TEM (XTEM) images. Figure 1 shows a comparison between the XTEM images of high Ge content GeSi alloys and GeSiC alloys. The $Ge_{0.8}Si_{0.2}$ alloy shown in Fig. 1(a) has some misfit dislocations at the interface and almost no planar defects within the thin film. With the addition of C, a significant increase in the number of planar defects (mainly twins and/or stacking faults) are observed, as seen in Fig. 1(b) for a $Ge_{0.76}Si_{0.2}C_{0.04}$ alloy film. In addition, the growth front of the GeSiC film is seen to be very rough [Fig. 1(b)] as compared to the equivalent GeSi alloy [Fig. 1(a)], consistent with the RHEED observations. Examples of XTEM images of low Ge content films are shown in Fig. 2. Figure 2(a) is an image from a $Ge_{0.6}Si_{0.4}$ alloy, while Figs. 2(b) and 2(c) are the images for $Ge_{0.59}Si_{0.34}C_{0.7}$ alloys with two different film thicknesses (30 and 70 nm). The growth front appears rough for the GeSiC

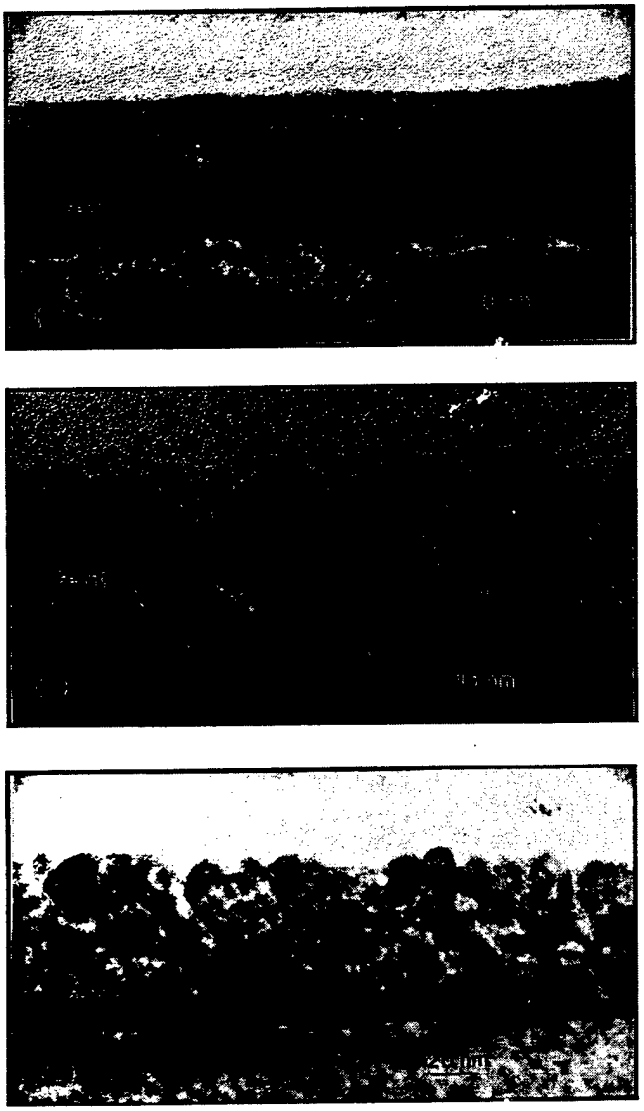

FIG. 2. XTEM images of (a) ~30 nm $Ge_{0.6}Si_{0.4}$ film showing smooth growth front, (b) ~30 nm $Ge_{0.59}Si_{0.34}C_{0.07}$ film, and (c) ~70 nm $Ge_{0.59}Si_{0.34}C_{0.07}$ film. (b) and (c) show rough growth front and an increased density of planar defects in the films compared with (a).

film in comparison to the GeSi film. However, the morphology of the thicker GeSiC film is not significantly different compared to the thinner film.

Statistical analyses were performed on the various XTEM images to obtain a rough estimate of the planar defect density as a function of C content, and are plotted in Fig. 3. The basic tendency is that the planar defect density increases with C content both for the Ge–C alloys and for the two groups of GeSiC alloys. *The addition of Si appears to enhance the tendency for planar defect formation.* This is evident from a comparison between Ge–Si–C alloy with ~4–7 at % C whose defect density is similar to Ge–C alloys with 10 at % C.[15] This implies that the addition of 20 at % or 40 at % Si does not improve the film quality under the conditions studied.

C. X-ray diffraction (XRD) studies

X-ray 2θ scans were performed in the (400) range for all the samples. The d_{400} ratio of the thin film alloy peak to that

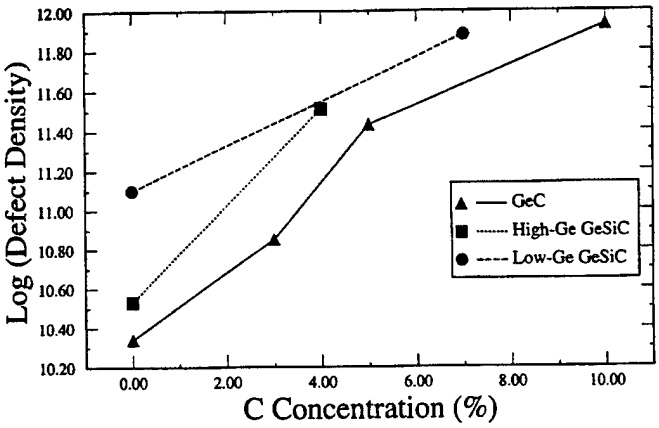

FIG. 3. Plot of planar defect density vs C concentration for Ge–C, type A (high Ge content) GeSiC and type B (low Ge content) GeSiC films. The rough estimation of the planar defect density in the films was obtained from XTEM images and is in the units of cm^{-2}.

of the Si substrate is plotted as a function of nominal C content in Fig. 4. The XRD data indicate that with increasing C content, the d_{400} spacing of the alloy films decreases, which suggests that C relaxes some of the compressive strain either by defect formation and/or by substitutional incorporation. If the equivalent GeSi thin film alloy is completely relaxed (assuming that the high temperature annealed sample is almost fully relaxed), the likely reason for GeSiC alloy thin film having a lower lattice parameter than GeSi is by C substitutional incorporation. The slope of the curve (which indicates the rate of substitutional C incorporation) appears to be similar for the high Ge content and the low Ge content alloys. The highest substitutional C incorporation is ~2.5 at % C (based on Vegard's law) and corresponds to the thicker (70 nm) $Ge_{0.59}Si_{0.34}C_{0.07}$ alloy film. An interesting point is that for the same composition, the thicker film appears to have a lower lattice parameter than the thinner film. Possible reasons will be addressed later.

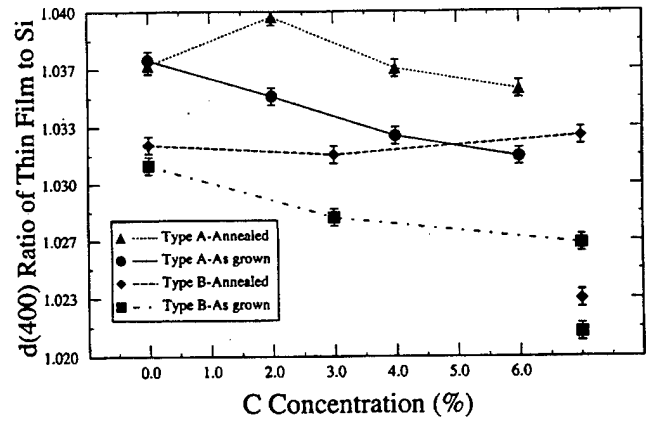

FIG. 4. The ratio of the (400) spacing of the film to that of the Si substrate (d_{film}/d_{Si}) plotted as a function of nominal C concentration for both type A (high Ge content GeSiC) and type B (low Ge content GeSiC) films in the as-grown and post-annealed conditions. The single solid box and solid diamond data points (showing the lowest value of d_{400}) are for the thicker low Ge content GeSiC films in the as-grown and post-annealed conditions.

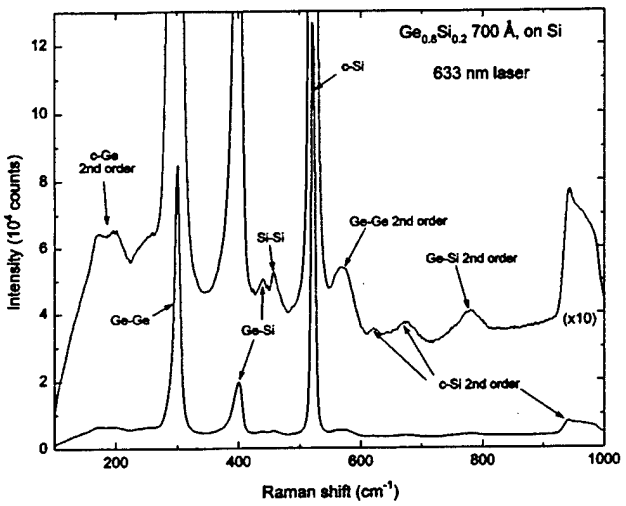

FIG. 5. Survey spectrum of a 70 nm $Ge_{0.8}Si_{0.2}$ epitaxial film on Si(100) obtained with 3 mW of 633 nm laser and 300 s exposure time.

D. Effect of annealing

Most samples were annealed *ex situ* in Ar atmosphere at 750 °C for 1 h. The XRD data (Fig. 4) show a small increase in the d_{400} spacings compared with the corresponding samples before the anneal. The change is however minimal for the GeSi samples (especially the $Ge_{0.8}Si_{0.2}$) suggesting perhaps that the as-grown sample is almost completely strain relaxed. It is also noted that the samples with the same composition ($Ge_{0.59}Si_{0.34}C_{0.07}$) but different thicknesses did not approach the same lattice parameter after the anneal. This result indicates that more C is incorporated in the thicker film than in the thinner film.

Another microstructural difference observed after annealing is that the XTEM images (not shown here) show that the misfit defect density at the interface has increased and the planar defect density within the film has decreased. This is true for both groups of GeSiC alloys. The microstructural effects of annealing Ge–C films on Si have already been published before.[15] The annealing causes Si to diffuse into the Ge–C layer as discussed in the following Raman spectroscopy section.

E. Raman spectroscopy

Figure 5 shows a typical unpolarized survey Raman spectrum of a 70 nm $Ge_{0.8}Si_{0.2}$ film. The main features in this spectrum have been discussed at length in previous studies.[17–25] The sharp peaks near 300, 400, and 500 cm^{-1} arise from the Ge–Ge, Ge–Si, and *c*-Si first-order modes, respectively. The remaining structure arises primarily from second-order scattering, as indicated in the figure. The film is sufficiently transparent at 633 nm that even the weak second-order features from the substrate are observable. Note that the second-order scattering from the Ge–Ge and Ge–Si modes of the film can be easily seen as can the first-order structure near 430 and 460 cm^{-1} associated with differing random environments around Ge–Si and Si–Si pairs, respectively.[19,22]

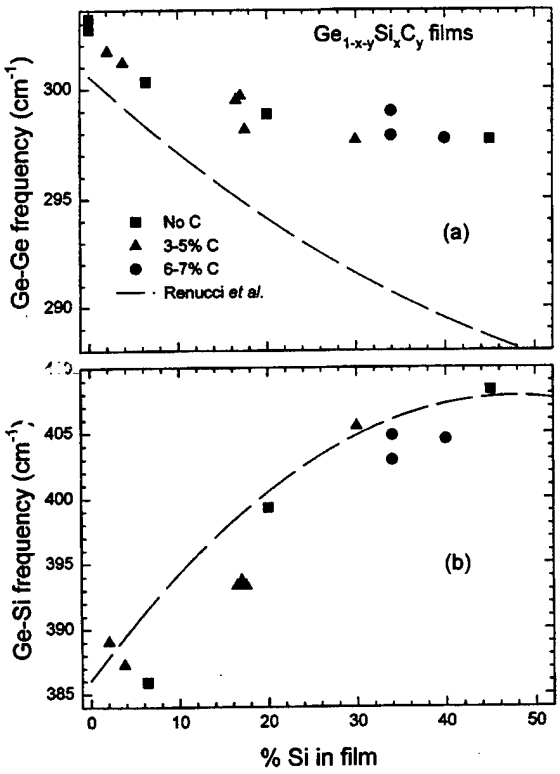

FIG. 6. Frequencies of the Ge–Ge and Ge–Si local modes as a function of the Si percentage in Ge–Si–C films on Si(100).

When C is added to a GeSi alloy we would expect systematic shifts of the primary Ge–Ge and Ge–Si modes in the film similar to those seen in Si-rich alloys by Meléndez-Lira *et al.*[26] and in $Ge_{1-x}C_x$ alloys by Yang *et al.*[15] Because of the low concentration of Si and interference from second-order substrate scattering, we are unable to see the Si–C local mode, which has been reported at 605 cm^{-1} in $Si_{1-x}C_x$.[5,27] The corresponding Ge–C local mode has not been previously seen, but its frequency can be estimated from the 605 cm^{-1} value using the following argument. The larger reduced mass of the Ge–C pair compared with Si–C will shift the frequency down by ~9.7%, and the larger Ge lattice constant will lead to an additional, smaller downward shift. Thus, the Ge–C local mode in Ge-rich alloys is expected to be in the 520–540 cm^{-1} region and will likely be obscured in the present study by the strong *c*-Si peak of the substrate. We have recently seen this mode at 529.8 cm^{-1} in $Ge_{1-x}C_x$ films grown on Ge(100) substrates, for which there is no interference.[28]

Figures 6(a) and 6(b) summarize the results on the Ge–Ge and Ge–Si mode frequencies for a large number of samples plotted as a function of the Si content. The spectra used for these data were done in the $z(xy)z^-$ scattering geometry, in order to reduce the second-order structure. The line frequencies in each case were determined by fitting with Pearson-type line shape functions, as described previously.[15] For comparison the trends observed for these frequencies in bulk, unstrained, polycrystalline alloys by Renucci *et al.*[17] are shown as dashed lines.

For the Ge–Ge frequency, shown in Fig. 6(a), there appear to be no obvious C effects. However, there is sufficient

scatter in the data that a small shift, of order $1-2\ \mathrm{cm}^{-1}$ as seen in $Ge_{1-x}C_x$ films,[15] cannot be ruled out. On the other hand, large positive shifts of $6-7\ \mathrm{cm}^{-1}$ seen in Si-rich alloys with fully strained, CVD-grown films can be ruled out.[26] As shown in Fig. 6(b) for the samples with nominal Si fractions of 20%–40%, C produces a negative shift of the Ge–Si frequency of a few cm^{-1}. This shift is opposite in sign and smaller in magnitude than the shifts seen for this mode in the CVD-grown film.[26] These differences are likely caused by differences in the strain as well as in the Ge fraction.

We have also included in Fig. 6 the results for $Ge_{1-x}C_x$ films into which Si has diffused during the annealing process.[15] The incorporation of Si in these films is demonstrated by the appearance of the Ge–Si local mode. The Si concentration has been estimated from the ratio of the integrated intensities of the Ge–Ge to Ge–Si lines. This ratio is expected to have a functional form $A(1-x)/2x$ for a random alloy. We first fit this form with data from the films with known Si content, obtaining the value $A=2.19$. Then the same value of A was used with the experimental intensity ratio to determine x for the films into which an unknown amount of Si had diffused. The resulting x values were 2%–6%. These are only rough estimates of x, since the Si concentration is not uniform. However, the general trend for these points as far as the dependence on Si % is the same as for the higher Si-content films.

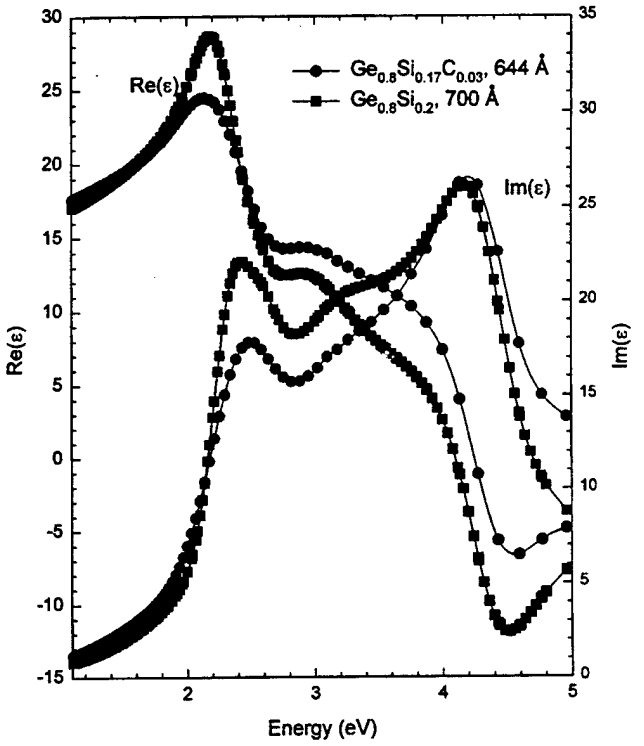

FIG. 7. Optical constants of GeSiC films on Si(100) obtained from spectroscopic ellipsometry results.

F. Spectroscopic ellipsometry

Spectroscopic ellipsometry measurements were made on the higher Si-content films for at least three angles of incidence in the range 60°–80° and covering the 1–5 eV energy range. Results are shown in Fig. 7 for films of nominal 20% Si content, with and without C; similar results are shown in Fig. 8 for films with ~40% Si. The linear increase in energy of the E_1 critical point (featured in 2–2.5 eV range) with increasing Si content is observed with all of our films. The slight energy shifts in the E_1 structure in Figs. 7 and 8 can be attributed to differences in Si content. The primary effect of C is a weakening of the structure near the E_1 point. This effect is observed in all films at all C concentrations and is consistent with our earlier observations on $Ge_{1-x}C_x$ samples.[14]

IV. DISCUSSION

A. Driving force for 3D growth

The XTEM images of GeSi alloys [Figs. 1(a) and 2(a)] showed that the growth fronts were planar, while the alloys with C show 3D growth morphology. The smooth morphology of GeSi alloys can be understood based on the argument that the only driving force for 3D island formation is strain energy relaxation, which is suppressed by a low growth temperature (~200 °C). This is consistent with our previous study of pure Ge on Si.[14,15] However, when C is present beyond a certain amount, the growth mode changes from 2D to 3D for both Ge–C and GeSiC thin films. As discussed in detail previously,[14,15] it is most likely that the presence of C (both in crystalline form and in the form of amorphous C) changes the surface energy such that Ge–C and GeSiC films find it unfavorable to wet the surface, leading to 3D island formation. From our RHEED observations, it is noted that the larger the fraction of nominal C in the flux, the sooner 3D

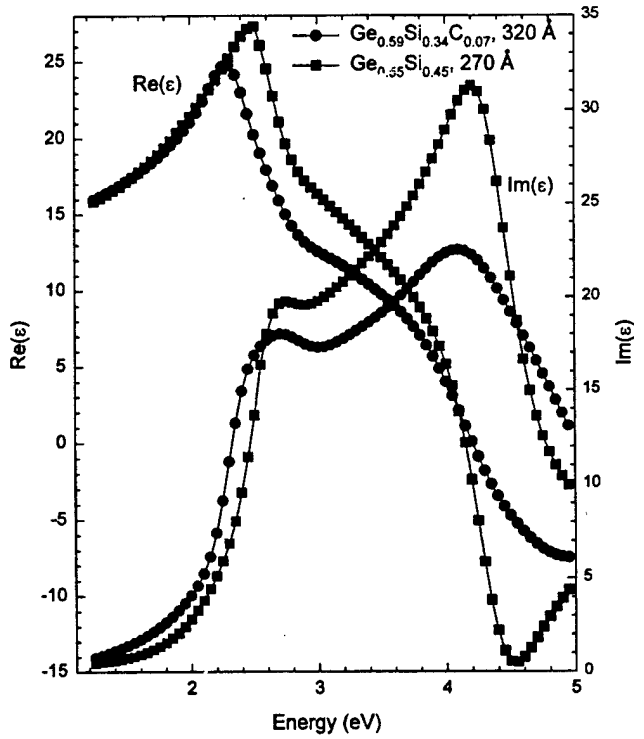

FIG. 8. Optical constants of GeSiC films on Si(100) obtained from spectroscopic ellipsometry results. The difference in the E_1 position of the two samples is primarily due to their different Si content.

islands tend to form. So it is conceivable that a larger driving force for 3D island formation (proportional to the amount of C) exists for SiGeC alloys such that island formation is observed even at such low substrate temperatures.

B. Formation of planar defects

From our experimental observation (Fig. 3), it is clear that under our growth conditions, both Ge–C and GeSiC alloy films form planar defects unlike pure Ge films on Si. Furthermore, the planar defect density increases with increasing C and Si concentrations and is more pronounced when both Si and C are present. The SiGeC alloys contain a higher planar defect density compared with equivalent Ge–C and GeSi films. Several possible origins of planar defect (especially stacking fault) formation have been suggested previously, including: the accommodation of misfit between coalescing islands,[29] nucleation of faults at heterogeneous SiC nanocrystallites,[13] or the formation of partial dislocations that move towards the surface, leaving stacking faults behind.[30] Our results suggest that the planar defect (stacking faults and twins) formation is closely related to the surface 3D morphology and therefore most likely to have formed from coalescence of islands. Furthermore, a clear correlation exists between increasing C content, 3D island density, and planar defect density.

The presence of Si in Ge–C amplifies the 3D growth morphology. We believe that the lower mobility of Si on the surface enhances 3D island formation and therefore increases the planar defect density. Such an idea is also consistent with our observation that high Si content GeSi films show more planar defects than low Si content films [compare Figs. 1(a) and 2(a)]. It is interesting to observe some similarities between the formation of planar defects in SiGeC films (especially the effect of Si) and low-temperature Si homoepitaxial growth (thickness-limited epitaxy).[31,32] It has been reported that surface roughening leads to the formation of facets and twins and eventual breakdown in crystalline epitaxy. While the origin of 3D growth is still unclear, effects such as step-edge barriers have been invoked at low growth temperatures.[31,32] We believe that such effects may also be contributing to the 3D growth in our films.

C. Incorporation of substitutional carbon

From the x-ray data (shown in Fig. 4), it can be noted that the d_{400} spacings of the Ge–Si–C alloys have a tendency to decrease with increasing C content. The decrease in the lattice parameter to a value lower than the almost fully relaxed GeSi (assuming the high temperature anneal results in near-complete relaxation of the GeSi alloy) suggests that C reduces the lattice parameter in the films by substitutional incorporation, which is consistent with other results, e.g.,.[4,12] The maximum amount of substitutional C is estimated to be ~2–3 at % based on the lowest value given in Fig. 4. This value is close to the data given by Refs. 6 and 10. The likely reason as to why the post-annealed samples have a higher lattice parameter than the as-grown samples, is that some substitutional C may have been ejected out from the films during high-temperature anneal.

D. Effect of film thickness

The interesting behavior of the samples with the same composition, but two different thicknesses (where the thicker film has a lower lattice parameter in both as-grown and annealed conditions) needs to be addressed. While the exact reason for this behavior is still unclear and further work is in progress, we suggest the following scenario. One possibility is that the thicker film is likely to have relaxed more strain than the thinner film. Consequently, the difference in the lattice parameter could be simply due to the larger residual compressive strain in the thinner film. Alternatively, it is possible that more substitutional C is incorporated during growth in the thicker film because of the lower strain in the film. We believe the latter effect is more likely because the lattice parameter of the post-annealed thicker film is still lower than the thinner film. We speculate that the C incorporation in such films may be a function of film thickness, which in turn is related to strain relaxation.

E. Effect of annealing

The annealing experiments at 750 °C show that the GeSiC alloys seem to have altered the microstructure, e.g., decreasing the planar defects density, leading to an improvement in the film quality. On the other hand, some substitutional C appears to have been ejected out from the film at 750 °C (based on the XRD measurements), which is undesirable. The reason for the ejection could be that this annealing temperature is outside the window for substitutional C incorporation,[16] thus the metastable thin film tends to relax by precipitating substitutional C.

V. SUMMARY

We have studied the epitaxial growth of two groups of Ge-rich GeSiC films by low-temperature MBE. The films were extensively characterized using RHEED, TEM, Raman spectroscopy, x-ray diffraction, and spectroscopic ellipsometry. While some amount of C (up to 2–3 at %) is incorporated in the GeSi alloys, excess C appears to cause 3D island formation and planar defects within the films. Increasing the amount of Si in the films enhances the tendency for planar defect formation, presumably due to lower mobility of Si atoms relative to Ge.

Raman spectra of alloy films show that the effects of C on the strong Ge–Ge local modes are far less than the effects due to Si. We are unable to observe any systematic change in the Ge–Ge mode, whereas the Ge–Si mode appears to shift to lower frequency with the addition of smaller C. Spectroscopic ellipsometry determinations of the film optical constants show that the primary effect of C is to reduce the strength of the E_1 critical point feature.

ACKNOWLEDGMENTS

The authors would like to thank Joe Mclaughlin for some help with TEM sample preparation and Barry Wilkens (ASU) for RBS measurements. Financial support for this research was provided by ONR Grant No. N00014-96-1-0793.

[1] J. C. Bean, Proc. IEEE **80**, 571 (1992).
[2] R. A. Soref, Proc. IEEE **81**, 1687 (1993).
[3] R. A. Soref, Z. Atzmon, F. Shaapur, M. Robinson, and R. Westhoff, Opt. Lett. **21**, 345 (1996).
[4] A. St. Amour, C. W. Liu, J. C. Sturm, Y. Lacroix, and M. L. W. Thewalt, Appl. Phys. Lett. **67**, 3915 (1995).
[5] J. Mi, P. Warren, M. Gailhanou, J.-D. Ganiere, M. Dutoit, P.-H. Jouneau, and R. Houriet, J. Vac. Sci. Technol. B **14**, 1660 (1996).
[6] C. L. Chang, A. St. Amour, and J. C. Sturm, Appl. Phys. Lett. **70**, 1557 (1997).
[7] Z. Atzmon, A. E. Bair, E. J. Jaquez, J. W. Mayer, D. Chandrasekhar, D. J. Smith, R. L. Hervig, and McD. Robinson, Appl. Phys. Lett. **65**, 2559 (1994).
[8] H. J. Osten, E. Bugiel, and P. Zaumseil, J. Cryst. Growth **142**, 322 (1994).
[9] A. R. Powell, K. Eberl, B. A. Ek, and S. S. Iyer, J. Cryst. Growth **127**, 425 (1993).
[10] J. Kolodzey, P. R. Berger, B. A. Orner, D. Hits, F. Chen, A. Khan, X. Shao, M. M. Waite, S. Ismat Shah, C. P. Swann, and K. M. Unruh, J. Cryst. Growth **157**, 386 (1995).
[11] B. A. Orner, J. Olowalafe, K. Roe, J. Kolodzey, T. Laursen, J. W. Mayer, and J. Spear, Appl. Phys. Lett. **69**, 2557 (1996).
[12] X. Lu and N. W. Cheung, Appl. Phys. Lett. **69**, 1915 (1996).
[13] H. J. Osten, Mater. Sci. Eng., B **36**, 268 (1996).
[14] M. Krishnamurthy, B.-K. Yang, and W. H. Weber, Appl. Phys. Lett. **69**, 2572 (1996).
[15] B.-K. Yang, M. Krishnamurthy, and W. H. Weber, J. Appl. Phys. **82**, 3287 (1997).
[16] H. J. Osten, M. Kim, K. Pressel, and P. Zaumseil, J. Appl. Phys. **80**, 6711 (1996).
[17] M. A. Renucci, J. B. Renucci, and M. Cardona, in *Proceedings of the Conference on Light Scattering in Solids*, edited by M. Balkanski (Flamarion, Paris, 1971), p. 326.
[18] J. Menéndez, A. Pinczuk, J. Bevk, and J. P. Mannaerts, J. Vac. Sci. Technol. B **6**, 1306 (1988).
[19] M. I. Alonso and K. Winer, Phys. Rev. **39**, 10 056 (1989).
[20] D. J. Lockwood and J.-M. Baribeau, Phys. Rev. B **45**, 8565 (1992).
[21] J. C. Tsang, P. M. Mooney, F. Dacol, and J. O. Chu, J. Appl. Phys. **75**, 8098 (1994).
[22] S. Gironcoli, Phys. Rev. B **46**, 2412 (1992).
[23] H. Rucker and M. Methfessel, Phys. Rev. B **52**, 11 059 (1995).
[24] Z. Sui and I. P. Herman, Phys. Rev. B **48**, 17 938 (1993).
[25] J. Zi, K. Zhang, and X. Xie, Phys. Rev. B **45**, 9447 (1992).
[26] M. Meléndez-Lira, J. Menéndez, W. Windl, O. F. Sankey, G. S. Spencer, S. Sego, R. B. Culbertson, A. E. Bair, and T. L. Alford, Phys. Rev. B **54**, 12 866 (1996).
[27] H. Rucker, M. Methfessel, B. Dietrich, K. Pressel, and H. J. Osten, Phys. Rev. B **53**, 1302 (1996).
[28] W. H. Weber, B.-K. Yang, and M. Krishnamurthy, Appl. Phys. Lett. **73** (in press).
[29] See, for example, M. J. Stowell, in *Epitaxial Growth, Part B*, edited by J. W. Matthews (Academic, New York, 1975).
[30] C. S. Ozkan, W. D. Nix, and H. Gao, Appl. Phys. Lett. **70**, 2247 (1997).
[31] D. J. Eaglesham, J. Appl. Phys. **77**, 3597 (1995).
[32] O. P. Karpenko, S. M. Yalisove, and D. J. Eaglesham, J. Appl. Phys. **82**, 1157 (1997).